



A novel oil palm frond magnetic biochar for the efficient adsorption of crystal violet and sunset yellow dyes from aqueous solution: synthesis, kinetics, isotherm, mechanism and reusability studies

Abdulrahman Adeleke Oyekanmi¹ · Kamil Kayode Katibi^{2,3} · Rohayu Che Omar¹ · Akil Ahmad⁴ · Moammar Elbidi^{5,6} · Mohammed B. Alshammari⁴ · Ibrahim Garba Shitu⁷

Received: 27 April 2023 / Accepted: 20 November 2023 / Published online: 9 January 2024
© The Author(s) 2024

Abstract

This study presented a facile synthesis route via the precipitation method for the production of magnetic biochar from oil palm frond (OPF). The physicochemical characteristics including surface, functional, and magnetic properties of the synthesized magnetic biochar revealed that the surface morphology, porosity, and magnetic properties enhanced its adsorption capacity for the removal of crystal violet (CV) and sunset yellow (SY) from aqueous solution. The saturation magnetization of OPF biochar was found to be 8.41 emu/g, coercivity (H_c) of 83.106 G, and retentivity (M_r) of 1.475 emu/g which implies that OPF magnetic biochar can be facilely separated from aqueous solution. The result also demonstrated superparamagnetic properties which provided suitable magnetic responsive characteristics to an external magnetic field. The interactive effect of the operational conditions of pH, adsorbent dosage, initial concentration, and temperature was investigated in a batch adsorption study using the central composite design (CCD) of the response surface methodology (RSM). It was indicated that an increase in adsorbent dosage to 1.0 g/L at a lower initial concentration (50 ppm) conducted at 20 °C favoured optimum removal of CV and SY at pH 11 and 4, respectively. The Langmuir isotherm model with maximum adsorption capacity (q_{\max}) of 149.03 and 342.47 mg/g was achieved for CV and SY dyes, respectively. The kinetic data proved to be best fitted to the pseudo-second-order kinetic model. Thermodynamic parameters revealed spontaneous and endothermic reactions. The suitability and sustainability of the magnetic biochar were enhanced by its regeneration potential for effective adsorption of CV and SY after 5 cycles which indicates its outstanding reusability. Hence, OPF magnetic biochar exhibited prospective application for the removal of dyes from wastewater.

Keywords Oil palm frond · Magnetic biochar · Crystal violet · Sunset yellow · Response surface methodology · Empirical modelling · Energy

✉ Kamil Kayode Katibi
kamil.katibi@kwasu.edu.ng

¹ Institute of Energy Infrastructure (IEI), Universiti Tenaga Nasional (UNITEN), Putrajaya Campus, Jalan IKRAM-UNITEN, 43000 Kajang, Selangor, Malaysia

² Department of Process and Food Engineering, Faculty of Engineering, Universiti Putra Malaysia (UPM), 43400 Serdang, Selangor, Malaysia

³ Department of Agricultural and Biological Engineering, Faculty of Engineering and Technology, Kwara State University, Malete 23431, Nigeria

⁴ Chemistry Department, College of Sciences and Humanities, Prince Sattam Bin Abdulaziz University, P.O. Box 83, 11942 Al-Kharj, Saudi Arabia

⁵ Department of Chemical and Environmental Engineering, Universiti Putra Malaysia, 43400 Serdang, Selangor, Malaysia

⁶ Department of Chemical and Petroleum Engineering, Faculty of Engineering, Elmergib University, Alkhoms, Libya

⁷ Department of Physics, Faculty of Science, Sule Lamido University, Kafin Hausa 700271, Jigawa, Nigeria

Introduction

One of the most persistent anthropogenic sources of environmental pollution is from the manufacturing sectors such as paper, printing, plastics, food, and textile industries thereby generating a considerable amount of effluents due to the consumption of dyes and water, especially during wet processing of textiles and food processing (Oyekanmi et al. 2019; Rizal et al. 2021). The negative environmental impact as a result of the presence of the residual dyes in aqueous solution is not limited to the poor aesthetic quality of the receiving water but can also create anoxic conditions that can be lethal to the resident aquatic population (Oyekanmi et al. 2022; Wang et al. 2023). The disposal of untreated dye wastewater has therefore become a matter of utmost concern due to the danger these dye pollutants pose to both the flora and fauna including the health of humans upon exposure (Nizam et al. 2022).

Crystal violet (CV) is one of the most common cationic dyes due to its intense colour which is extensively used in textile, paper, and printing ink industries (Sabna et al. 2016); therefore, a low concentration of CV in the solution can distort sunlight penetration and also photosynthetic activities (Mittal et al. 2021). This dye is also known to be carcinogenic; its exposure can potentially be detrimental to the health of humans and other life forms (Ahmad & Ansari 2022). Sunset yellow (SY) is one of the most used synthetic dyes in the food industry mostly used as a food additive in beverages, dairy candies, and bakery products. Consequently, it becomes necessary to decontaminate dye effluents before they are discharged into the natural and unpolluted water bodies. Thus, sustainable cost-effective treatment strategies are urgently required to control the harmful effects of these dyes in order to preserve the ecosystem.

Conventionally, decontamination techniques which include ion exchange, reverse osmosis membrane, nanofiltration membrane, solvent extraction, photocatalytic degradation, and adsorption have been widely applied for the treatment of dyeing effluent (Ahmadipouya et al. 2022; Katibi et al. 2021; Kumar 2019; Saeki et al. 2021; Thasneema et al. 2021; Wang et al. 2021). Even though these methods are technically viable when suitable materials are used, the cost implication of the treatment process is relatively high, unlike the adsorption method which is known for its simple operation, high treatment efficiency, and environmental friendliness without causing secondary pollution (Li et al. 2022; Jie et al. 2023).

Recently, the synthesis of biochar as a potential adsorbent for the remediation of pollutants from wastewater streams has been receiving much attention due to its high porosity, enhanced surface area, and abundance of active

functional groups (Zhang et al. 2021; Hu et al. 2022). However, the major challenge of post-adsorption processes such as filtration or centrifugation in terms of separation and recovery especially biochar in powdered form remains a drawback that limits its wider application (Jung et al. 2016; Mahdi et al. 2018; Fito et al. 2023). Therefore, to proffer a solution to this problem to advance its application for pollutant removal, surface modification via iron oxide precipitation has been proposed to enhance the adsorption capacity and ease the post-adsorption recovery and separation. Several modification techniques to enhance the physical, chemical, and biological properties of biochar using biofilms, clays, and metal salts have been reported (Akgül et al. 2019; Frankel et al. 2016; Xing et al. 2021; Yao et al. 2014). To reduce the cost of synthesizing magnetic biochar, agricultural wastes can be utilized as a precursor for biochar preparation. In this study, a facile synthesis method has been proposed for the preparation of Na_2CO_3 magnetic biochar for the adsorption of dyes.

Oil palm frond (OPF) could be utilized as a potential raw material to prepare biochar because it is easily sourced waste biomass. It is estimated that about 24 fronds are pruned per palm tree on an annual basis. Most of the OPF biomass are underutilized and are left rotting between the rows of palm trees and the weight of OPF varies considerably with the age of the palm having an average annual pruning of 82.5 kg of fronds/palm/year (Harith Zafrul Fazry et al. 2018). Oil palm mill wastes generate greenhouse gases (CH_4 , CO_2) which can affect the environment, especially air and water resources (Khatun et al. 2017). Annually, approximately 26.2 million tonnes of oil palm frond (OPF) are generated through the oil palm production process in oil mills (Singh et al. 2013; Dong et al. 2022). However, not all OPF residues are utilized for energy applications, they can be a source of greenhouse gas emissions (Isgiyarta et al. 2022). Massive accumulations of biomass pose environmental pollution issues as a result of the high concentration of organic acid in the OPF (Jasri et al. 2023). Burning OPF wastes emit air pollutants harmful to health and the environment (Nordin et al. 2017). Rather than OPF becoming a potential threat and source of environmental pollution, this waste can be utilized as an economically viable raw material for the synthesis of biochar to achieve high surface area adsorbent for pollutant remediation. However, by enhancing the adsorption capacity of biochar by improving its surface properties and enhancement of its effective surface functional groups, magnetically modified biochar has gained considerable attention for pollutant removal (Eltaweil et al. 2020). Nevertheless, most methods of modification such as

acid–base activation are usually broad without significant effect on the improvement of pore structure and surface properties of the adsorbent (Li et al. 2022). The synthesis of magnetic biochar derived from OPF offers a novel interfacial surface and enhanced structure for the adsorption of dyes from the solution. Pristine biochar tends to rely on its hydrophobicity in the aqueous phase (Sun et al. 2022). However, loss of adsorbent and the issue of secondary pollution due to desorption limit biochar applications. The recovery of biochar using an external magnet source provides an easy and effective regeneration route (Rubangakene et al. 2023). Oil palm frond have inherent lignocellulosic properties. It is expected that the cellulose composition of OPF to provide a wide functionalizable surface which can enable the incorporation of functional groups onto the surface, thereby enhancing the adsorption capacities of the surface towards pollutant removal (Othmani et al. 2021). Furthermore, the lignin content comprises various functional groups which include carbonyl, carboxyl, methoxy, and hydroxyl groups, which offers promising potential for dye adsorption (Meng et al. 2020).

Furthermore, investigating the interaction of the operational adsorption parameters in a batch adsorption study intends to increase the adsorption capacity of the magnetic biochar for dye removal from an aqueous solution. There have been many studies on magnetic biochar using CCD and RSM. So far, phenol contaminated municipal wastewater treatment using date palm frond biochar optimization using response surface methodology has been reported. From our literature survey, magnetic biochar derived from oil palm frond has rarely been synthesized for pollutant remediation. Our study conducted a facile synthesis of OPF magnetic biochar for the adsorption of crystal violet and sunset yellow dye which has not been reported in the literature. Furthermore, the synergistic interaction of process variables influencing the adsorption capacity of adsorbent through optimization of operational parameters using CCD-RSM was conducted in our study which will provide valuable insight into the synthesis of OPF magnetic biochar as an effective adsorbent for the removal of pollutant species from solution.

Herein, OPFs were utilized as precursory material for the synthesis of novel functionalized Na_2CO_3 -based magnetic biochar which was applied for the adsorption of CV and SY from an aqueous solution. In addition, this work intends to explore the effect of the system parameters for the adsorption of CV and SY on the magnetic biochar using experimental design and optimization of operational variables using the central composite design (CCD) approach of the response surface methodology (RSM) and to study

the isotherm, kinetic and thermodynamics of the adsorption process including its regeneration potential.

Materials and method

Preparation and characterization of OPF magnetic biochar

Materials

All chemicals and reagents used in this study were of analytical grade. Distilled water was used for the preparation of all aqueous solutions throughout the experiment. Sodium carbonate (Na_2CO_3), ethanol ($\text{C}_2\text{H}_5\text{OH}$), Iron (III) chloride (FeCl_3), and iron sulphate (FeSO_4) were procured from Sigma-Aldrich Co. (MO, USA) and utilized without additional purification. The raw oil palm frond used in this study was obtained from West Palm Oil Mill in Sime Darby Sdn. Bhd., Carey Island, Selangor, Malaysia. The feedstock was collected and oven-dried at 95°C overnight after which it was kept in a dry air-tight glass jar at ambient temperature before subsequent procedures.

Synthesis of OPF magnetic biochar

Oil palm frond (OPF) was initially washed using distilled water repeatedly to expunge unwanted foreign materials and other impurities. The OPF biochar was prepared by the pyrolysis method. Then, 20.0 g of washed oil palm frond OPF precursor was primarily pyrolyzed between 200 and 600°C for 3 h under the nitrogen (N_2) gas condition at 230 mL/min after which the heater temperature was steadily increased for 60 min at a rate of $5\text{--}10^\circ\text{C}/\text{min}$ and was enabled to cool (within 120–180 min) even under N_2 flow to ambient temperature after initially being held at 500°C for 60 min. Afterwards, the OPF biochar was milled using a high-energy ball milling technique for 3 h, sieved to a particle size $< 60\ \mu\text{m}$, and rinsed with distilled water and ethanol four times to eliminate impurities. The rinsed OPF biochar was oven-dried at 110°C for 24 h and then kept in airtight 80-mL borosilicate glass vials prior to further use. Next, 12.5 g of the dried OPF biochar was soaked in a solution containing 100 mL of $0.125\ \text{mol}\cdot\text{L}^{-1}$ of FeSO_4 and FeCl_3 of $0.25\ \text{mol}\cdot\text{L}^{-1}$ solution was uniformly stirred via the magnetic stirrer. The mixture was further subjected to heat at 60°C with steady stirring to allow successful saturation of Fe^{2+} and Fe^{3+} into OPF biochar and subsequently allowed to cool to 40°C . Then, 10 mol/L sodium carbonate (Na_2CO_3) solution was dropwise added to the mixture under robust magnetic stirring, to raise the suspension pH to 10–11, and

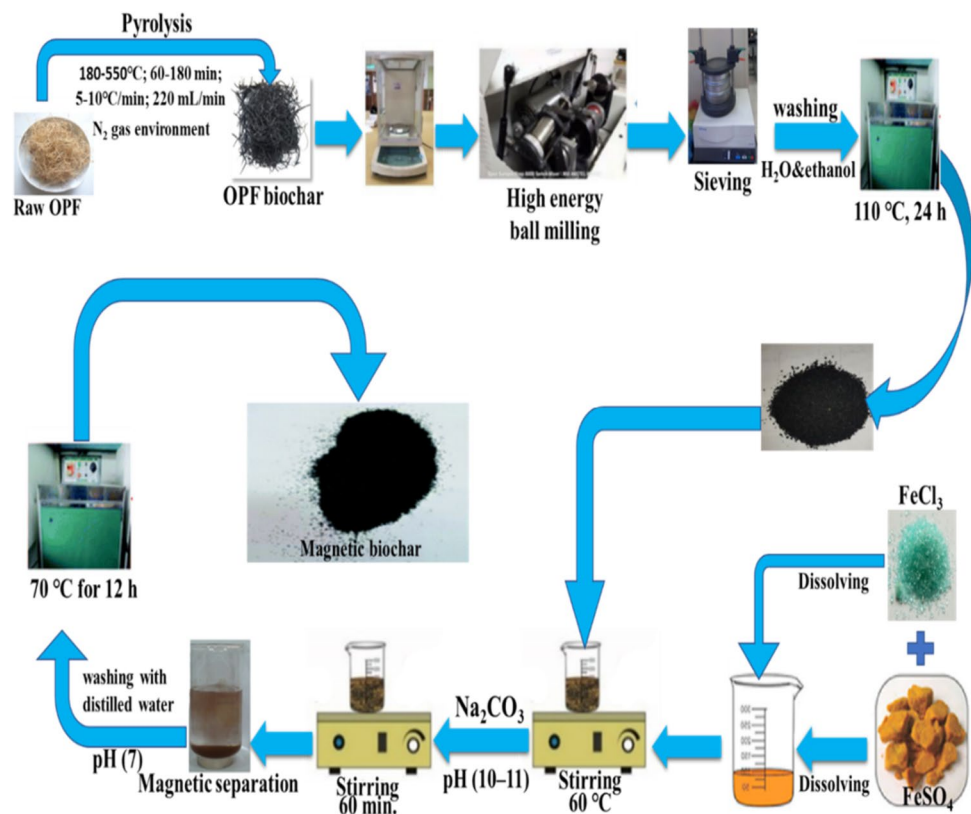
the solution transformed from brownish green to black. Fe_3O_4 precipitation was developed on the surface of biochar materials under alkaline conditions. Upon the completion of the reaction, the Na_2CO_3 -saturated biochar solution was sufficiently stirred for 60 min to attain a homogenous mixture and better dispersion. The resultant solution was separated using an external magnet and washed with distilled water to alter the solution pH to 7 and then dried at 70 °C for 12 h. The final obtained samples were stored in sealed containers and utilized during the adsorption experiments and in the biochar characterization. The synthesis route for the production of magnetic biochar from OPF as precursory material is illustrated in Fig. 1.

Characterization of OPF magnetic biochar

The surface properties of the magnetic biochar were examined using the N_2 vapour adsorption/desorption method to determine its effective surface area, pore volume, and pore diameter at 77 K using a nano-porosity system (NP-XQ, Mirae Scientific Instruments, South Korea). The morphology at the surface of the Na_2CO_3 magnetic biochar was obtained using scanning electron microscopy, Hitachi S2300 model which was conducted at 25 kV accelerating voltage. The elemental composition of the surface

properties was obtained using a scanning electron microscope equipped with energy-dispersive X-ray spectroscopy (SEM–EDS, Inspect F, FEI Co., USA) analyser. Before SEM–EDX, the test samples were carbon-coated using an Edwards Scancoat machine to reduce the possibility of a charging effect. The degree of crystallinity of the magnetic biochar was evaluated using X-ray diffraction (XRD, D8 Advance Sol-X, Bruker Co., USA). The surface functional properties of the magnetic biochar were investigated using a Fourier transform infrared (FT-IR) spectrometer, (NICOLET iS10, Thermo Scientific, USA). A test sample was used to examine the magnetic moment of Na_2CO_3 magnetic biochar conducted at room temperature using a vibrating sample magnetometer (VSM, Lake Shore Cryotronics, USA). The functional groups were obtained from the FT-IR spectra in the range of 4000–400 cm^{-1} . X-ray diffraction (XRD) was used to investigate the chemical and phase composition of the synthesized biochar adsorbents at Cu $\text{K}\alpha$ radiation (2θ spectrum = 20–80°; phase = 0.05° 2θ ; time per step = 0.2 s) via X-ray powder diffractometer (Philips, X'pert Pro PANALytical PW3040 MPD). The specific surface area, pore width, and pore volume of the OPF biochar and the magnetic biochar were obtained, respectively, using the Brunauer–Emmett–Teller (BET) (Micromeritics ASAP 2020 system, USA).

Fig. 1 Synthesis of OPF magnetic biochar



Batch adsorption studies

Synthetic dyes procured from MP Bio-medicals, LLC of high purity grade (> 99.9%) which are CV(C₂₅N₃H₃₀Cl) and SY(C₁₆H₁₀N₂Na₂O₇S₂) having a molecular weight of 407.979 and 452.37 g/mol, respectively, were used as model adsorbate. The chemical structures of CV and SY are illustrated in Fig. 2. In the study, 1000 mg/L stock solution was prepared in a volumetric flask by dissolving 1.0 g/L of the respective dyes with deionized water to obtain the desired concentrations. Static equilibrium adsorption experiments were performed in a thermostat shaker model HZ-9211 K which was set to 150 r/min at temperature intervals according to the experimental design. The adsorption kinetic study was conducted at a predetermined time interval based on the optimized time condition from the experimental run. At the end of the equilibrium time, the supernatants were drawn for content investigation.

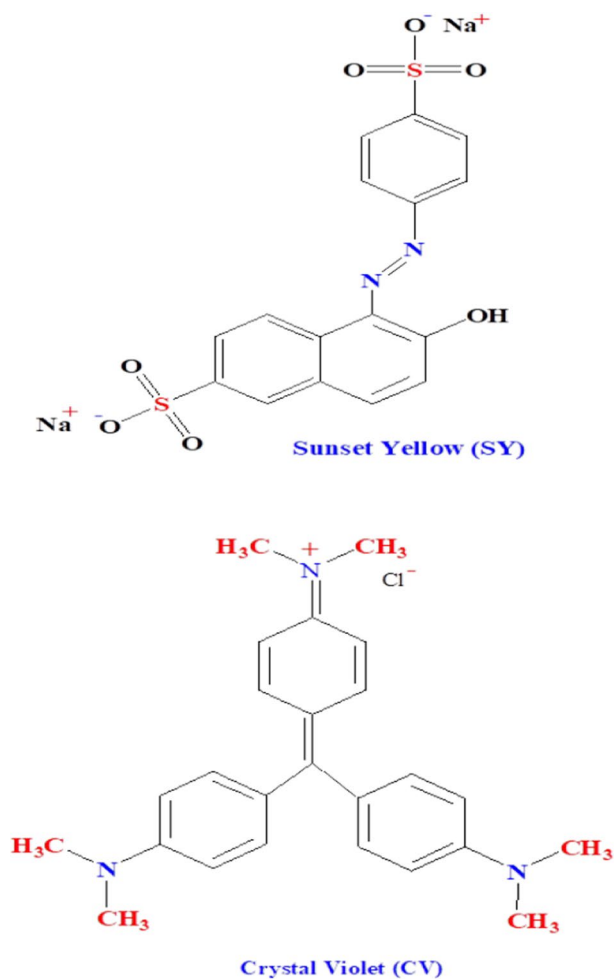


Fig. 2 Chemical structure of CV and SY dyes

The adsorption capacity at equilibrium (q_e , mg/g) was evaluated from the mass balance equation according to the equation [1].

$$q_e = \left(\frac{C_i - C_f}{m} \right) V \quad (1)$$

where C_i and C_f denote the initial and residual dye concentrations (mg/L), respectively, V is the volume of the dye solution (L), and M indicates the weight of the adsorbent (g).

RSM-CCD experimental design and process optimization

The effect of operational variables was determined through batch study to determine the adsorption efficiency of the magnetic biochar for the removal of CV and SY. The effect of pH, initial concentration, and contact time was investigated using the central composite design (CCD) of the response surface methodology (RSM) (JMP Pro 12.2 software, SAS Institute, Inc.). The experimental design showing the low, medium, and high levels of each design variable used to generate a table of experimental runs is presented in Table 1. This is to evaluate the relationship between the process variables as a function of the per cent removal of dyes investigated using a second-order degree polynomial equation. The variables are denoted accordingly as initial concentration (X_1), pH (X_2), contact time (X_3), and temperature (X_4). On the basis of this matrix, 30 experimental runs were generated. The experiments were carried out according to the matrix design given by the CCD as an expression for the responses (% dye removal). The interaction of the independent variables is represented using a response surface equipped with the CCD to establish the relationship of the complex function of the responses according to Eq. (2).

$$Y = \beta_0 + \sum_{i=1}^K \beta_i X_i + \sum_{i=1}^K \beta_{ii} X_i^2 + \sum_{i>j}^K \sum_{j>i} \beta_{ij} X_i X_j + \epsilon \quad (2)$$

where β_0 and β_i signify the constant coefficient, and X_i represents the linear coefficient of the input parameters. β_{ii} denotes the quadratic coefficient of the input

Table 1 Design matrix for CCD: variables, domain, and design interval

Variables	Factor code	Level of factors		
		Low (-1)	Central (0)	High (+1)
pH	X_1	4	7.5	11
Adsorbent dosage	X_2	0.5	0.75	1
Initial concentration	X_3	50	100	150
Temperature	X_4	20	30	40

parameter, X_i , β_{ij} is the interaction coefficient between the input parameter X_i and X_j , and ϵ shows the error of the model.

Equilibrium kinetics, isotherm, and thermodynamic studies

To study the kinetics of adsorption of CV and SY on magnetic biochar, four kinetic models were used for the expression of adsorption properties of the magnetic biochar for the removal of CV and SY. The models are the pseudo-first-order model, pseudo-second-order model, Elovich, and intraparticle diffusion model.

The pseudo-first-order and pseudo-second-order equations are given by (7) and (8), respectively.

Pseudo-first-order model:

$$\ln(Q_e - Q_t) = \ln Q_e - k_1 t \quad (3)$$

Pseudo-second-order model:

$$\frac{t}{Q_t} = \frac{1}{K_2 Q_e^2} + \frac{1}{Q_e} t \quad (4)$$

Q_e represents equilibrium adsorbate concentration, Q_t expresses the amount of adsorbate adsorbed at time t , and k_1 (1/min) and k_2 (g/(mg min)) are the adsorption rate constants.

Elovich's model assumed that equilibrium occurs over a long period without giving an account of the rate of desorption. The linearized form of the equation is given by Eq. (5).

Elovich model:

$$q_t = \frac{1}{\beta} \ln \alpha \beta + \frac{1}{\beta} \ln t \quad (5)$$

where α indicates the initial adsorption rate (mg/g min), and β is the desorption constant. The slope $1/\beta$ and the intercept represent $\ln(\alpha\beta)/\beta$ were obtained from the plot of $\ln t$ versus q .

The mechanism of interaction of the adsorbent and adsorbate was determined using the intraparticle diffusion model according to Eq. (6).

$$\text{Intraparticle diffusion model} : = q_t + k_i t^{0.5} + c \quad (6)$$

where q_t is the amount of adsorbed CV and SY, k_i is the rate constant of the intraparticle diffusion model (mg/g min^{0.5}), and c is the intercept.

The interpretation of the equilibrium process is important to establish the relationship between the analyte and the bio-adsorbent under different experimental conditions. This is to provide an appropriate outline for an optimum operational procedure. In this study, the Langmuir, Freundlich, Temkin, and Dubinin–Radushkevich isotherm

models were used to fit equilibrium isotherm data to analyse the adsorption of CV and SY dyes adsorbed on the interface of the magnetic biochar.

The Langmuir isotherm is denoted by:

Langmuir isotherm:

$$\frac{1}{q_e} = \frac{1}{q_m} + \frac{1}{K_L q_m C_f} \quad (7)$$

where q_m describes the maximum monolayer adsorption capacity (mg/g), and q_e represents the equilibrium biosorption capacity of CV and SY adsorbed on the magnetic biochar. C_f is the equilibrium of dye concentration (mg/L), and K_L indicates the Langmuir constant (L/mg).

The Freundlich isotherm is denoted by:

Freundlich model:

$$\log q_e = \log K_f + \frac{1}{n} \log C_f \quad (8)$$

where q_e represent equilibrium biosorption capacity of CV and SY adsorbed on the magnetic biochar K_f indicates the Freundlich constant indicating the degree of adsorption ((mg/g) (L/mg) 1/n), 1/n denotes the adsorption capacity, and C_f represents the Equilibrium concentration of CV and SY in solution (mg/g).

The Temkin isotherm is denoted by:

Temkin model:

$$q_e = B \ln A + B \ln C_f \quad (9)$$

where $B = RT/b$, b indicates the Temkin constant related to the heat of sorption (J/mol); A represents the Temkin isotherm constant (L/g), R is the gas constant (8.314 J/mol K), and T is the absolute temperature (K). The constants A and b can be obtained from the plot of q_e against $\ln C_f$.

The Dubinin–Radushkevich isotherm is represented by:

Dubinin–Radushkevich model:

$$\ln q_e = \ln q_m - \beta \epsilon^2 \quad (10)$$

where β and ϵ represent the model parameters, $\epsilon = RT \ln(1 + \frac{1}{C_f})$, the adsorption process's free energy is given by:

$$E = \frac{1}{\sqrt{2\beta}}$$

The thermodynamic constants were used to determine the effect of temperature on the rate of adsorption of CV and SY on the magnetic biochar which was derived from the Van't Hoff equation. The thermodynamic parameters which were the Gibbs free energy of adsorption (ΔG°), entropy (ΔS°), and enthalpy (ΔH°) changes were evaluated for the CV and SV dye adsorption data at a temperature interval of 293–303 K. The parameters were represented by Eqs. 11–13, respectively.

$$\Delta G^\circ = -RT \ln K_d \quad (11)$$

$$\Delta G^\circ = \Delta H^\circ - T\Delta S^\circ \quad (12)$$

$$\ln K = \frac{\Delta S^\circ}{R} - \frac{\Delta H^\circ}{RT} \quad (13)$$

where R (8.314 J/mol K) represents the universal gas constant, T (°K) denotes the absolute temperature, and K_d defines the dissociation constant.

Regeneration study of magnetic biochar

To carry out the regeneration study, the saturated magnetic biochar was contacted separately with (0.1 mol/L) 0.1 M HCl, methanol, and NaOH as eluting agent. The adsorbed CV and SY were desorbed under 2 h at an agitation speed of 150 rpm conducted at 25 °C. After separating the magnetic biochar from the solution, the CV and SY concentration in the supernatant was analysed. The filtered analytes were investigated using a visible spectrophotometer (PerkinElmer Lambda 25 UV/VIS spectrophotometer) to determine the residual dye concentration. For each of the removal cycles under optimal conditions, the magnetic biochar was washed twice with deionized water before the next cycle. The desorption efficiency of the magnetic biochar in terms of CV and SY was evaluated according to Eq. (14).

$$\text{Desorption efficiency (\%)} = \frac{\text{Amount of dye desorbed}}{\text{Amount of dye adsorbed}} \times 100 \quad (14)$$

Results and discussion

Physicochemical characteristics of biosorbents

Elemental dispersive X-ray (EDX) analysis of the synthesized pristine OPF biochar (neat biochar) and the magnetic biochar is presented in Table 2. The EDX spectra are shown in Fig. 1. The elemental composition of C and O in terms of atomic percentage featured predominantly in both the neat and magnetic biochar. It was indicated that the neat biochar exhibited higher total carbon contents (85.60%) which can better be explained as a result of high pyrolysis temperature (500 °C) which tends to form a higher degree of carbonization (Zhao et al. 2019; Wang et al., 2020). Conversely, magnetic biochar was seen to

be composed of higher oxygen atoms by 35.31% (Khan et al. 2020). Presumably, more oxygen functional groups on the surface of the magnetic biochar relative to the starting material create the possibility of enhanced adsorption capacity. Notably, the increase in Fe content compared to 0% Fe content in the pristine biochar indicated successful modification of the magnetic biochar and also revealed the incorporation of Fe in the biochar matrix.

The surface morphology of the phases of biochar transformation was obtained using SEM analysis. As shown, Fig. 3a–d illustrated the SEM images of pristine OPF biochar, magnetic OPF biochar before adsorption, magnetic biochar after adsorption of SY, and magnetic biochar after adsorption of CV, respectively.

The structure of pristine OPF biochar (Fig. 3a) exhibited a smooth and porous surface as compared to the surface of magnetic biochar which was expectedly rough, compact, and tightly packed as a result of rich microparticles originating from the accumulation of Fe which was incorporated in the surface of the biochar. The surface of magnetic OPF biochar developed a considerable amount of pore channels as well as interior mesopores as shown in Fig. 4b, providing sites for the binding effect of dye molecules on its surface. The formation of a series of cavities over the surface of OPF was linked to the breakdown of lignocellulosic biomass at elevated temperatures, causing the evaporation of volatile compounds from the freshly formed pores (Arafat Hossain et al. 2017; Kong & Liu 2021). Figures 3c, d illustrated that the surface of OPF biochar was clustered and covered by attachments which were further proven to be iron oxide by the EDX analysis and revealed the binding of dye molecules of CV and SY on its surface samples following the adsorption test. A significant number of nanoparticles were discarded on a porous biochar surface. It is expected that during the adsorption process, the dyes were trapped onto the surface of biochar and the iron (Fe) nanoparticles strengthened the attachment through the interaction with the dye molecules.

The hysteresis loops of OPF magnetic biochar were determined using VSM magnetic measurement system under room temperature to evaluate the magnetic behaviour of OPF magnetic biochar. As demonstrated in Fig. 4, the characteristic saturation magnetization of OPF magnetic biochar was found to be 8.41 emu/g, which implies that OPF magnetic biochar can be facilely separated from an aqueous solution using an external magnetic field. Also, coercivity (H_c) and retentivity (M_r) of 83.106 G and 1.475 emu/g, respectively, revealed that OPF magnetic biochar demonstrated superparamagnetic properties at room temperature and was able to offer suitable magnetic responsive characteristics to an external magnetic field. Therefore, the potential of the OPF biochar to be readily recollected from the aqueous solution by applying the external magnetic field makes its reusability possible in the real wastewater treatment process.

Table 2 Elemental analysis of the OPF biochar (wt%)

Samples	C	O	Si	Fe	Total (wt%)
Neat biochar	85.60	14.08	0.31	0	100.00
Magnetic biochar	47.74	35.31	0.30	16.65	100.00

Fig. 3 Surface morphology of **a** OPF, **b** magnetic biochar **c** Adsorption of CV on magnetic biochar **d** Adsorption of SY on magnetic biochar

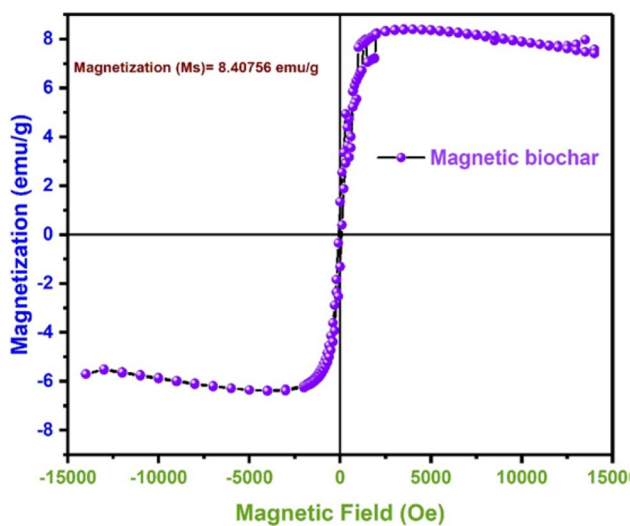
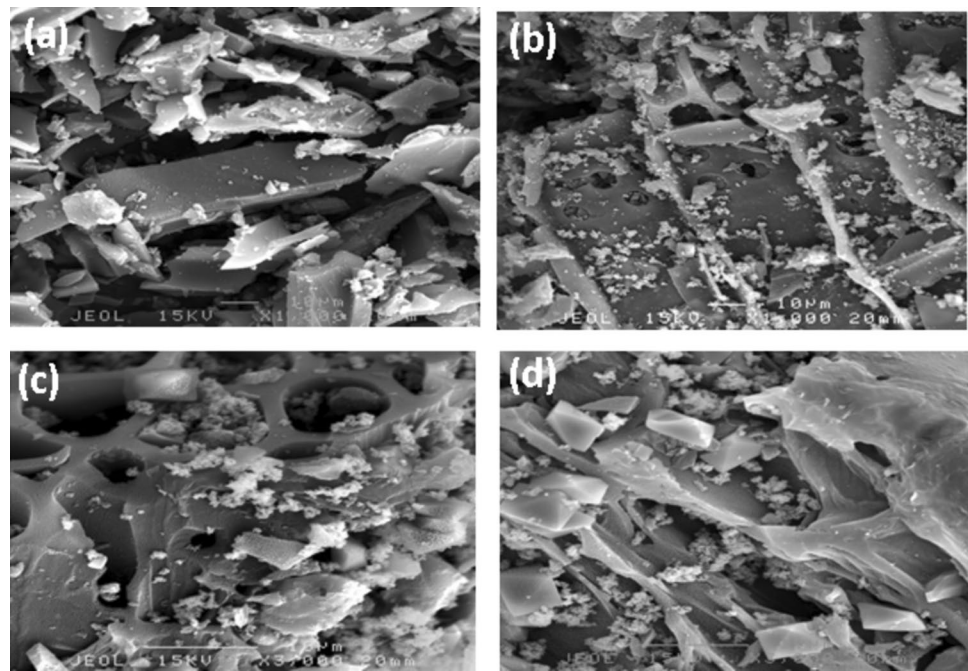


Fig. 4 Magnetic properties analysis of OPF

The surface properties were obtained using the assessment of the functional group profiles of OPF biochar and magnetic biochar via FTIR spectra analysis. The predominant functional groups which include C=O, C–OH, C=C, and –OH were dominant features of the adsorbents. In Fig. 5a, the broad peaks around 3800–3000 cm^{-1} and the peak around 1250 cm^{-1} denote the presence of hydroxyl and carboxyl groups, respectively, on the surface of the OPF biochar (Zahedifar et al. 2021). The stretching frequency at 2349 cm^{-1} shows the presence of NH_2 symmetric stretching. The peaks at 1740.29 cm^{-1} are assigned to the stretching

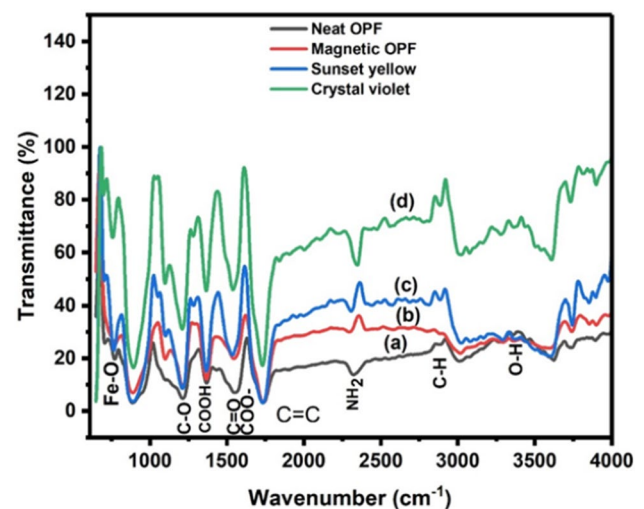


Fig. 5 Surface functional groups on **a** Neat biochar **b** magnetic biochar **c** adsorption of CV **d** Adsorption of SY

vibration of C=C in aromatic rings. The characteristic peaks around 580 and 753 cm^{-1} typically represent Fe–O, indicating the deformation in the hexagonal sites of iron oxide (Feng et al. 2023) (Fig. 5b). There was no noticeable shift in the FT-IR spectra attributed to C–O groups before and adsorption of CV and SY dye in Fig. 5b and C. The band intensity of COOH decreases after the adsorption of the dyes molecules, respectively, indicating that favourable adsorption occurred as a result of electrostatic interaction between the COOH group on the surface of the magnetic biochar and the dye molecules (Molla et al. 2019).

X-ray diffraction analysis illustrates the nature of the planes and size of a material (Shitu et al. 2023). The crystalline structures of both the neat and magnetic OPF biochar were examined using XRD diffraction spectra. The X-ray diffraction patterns (XRD) of neat and magnetic OPF biochar were in the range of 20–80° are shown in Fig. 6. The diffraction spectra of the synthesized neat OPF biochar showed the existence of hematite (Fe₂O₃). The diffraction peaks of neat OPF biochar at 2θ were 18.48° and 44.56° indexed to the (003) and (104) hkl planes, respectively, which corresponds to standard card Inorganic Crystal Structure Database (ICSD No. 98–006–4887). The OPF magnetic biochar exhibited diffraction peaks at 2θ of 24.15°, 33.18°, 35.62°, 40.87°, 49.48°, 54.11°, 62.45°, and 72.05° which were found to be indexed to the (012), (104), (110), (113), (024), (116), (214), and (1010) hkl planes, respectively, corresponding satisfactorily with the database of Fe₂O₃ standard card Inorganic Crystal Structure Database (ICSD No. 98–010–4924) with lattice parameter (a=b=c) of 23.8012 Å with a space group of R-3 m and substantiates the signature peaks of a hexagonal unit cell Fe₂O₃, respectively, with no impurity peak in the XRD pattern noticed. This signifies that the Fe₂O₃ particles were favourably crystalline hexagonal spinel structures. There were no other peaks associated with another material detected from the XRD result, which confirmed that the nano-magnetite was pure hematite (Fe₂O₃). The XRD spectra of Fe₂O₃ indicated that both Fe₂O₃ and neat OPF biochar patterns overlapped in the XRD spectra of OPF magnetic biochar, indicating successful synthesis of OPF magnetic biochar. This suggested good agreement with the FT-IR result signifying the successful incorporation of

Fe₂O₃ nanoparticles in the matrix of the OPF biochar (Feng et al. 2023; Shitu et al. 2020).

The textural properties of the OPF biochar and the magnetic biochar were obtained from the BET analysis. It was revealed that the major physical factors influencing the adsorption of CV and SY were the specific surface, pore volume, and pore width of the magnetic biochar as shown in Table 3. Relative to the pristine biochar, the specific surface area of the magnetic biochar decreased. This was indicated in the S_{BET} of 280 m²/g, 0.042 as exhibited by the OPF biochar compared to the magnetic biochar (162.1998 m²/g). The specific surface area of the magnetic biochar was expected to decrease, this was attributed to the high carbonaceous surface area and its surface area composed of Fe₃O₄ (Li et al. 2019). The result was in agreement with the previous study (Zhou et al. 2018).

The N₂ adsorption/desorption isotherms for OPF biochar and magnetic biochar are illustrated in Fig. 7. It was revealed that the pristine biochar and the magnetic biochar exhibited type I V curves. From Fig. 7a, a slow steady increase in the amount of adsorption was achieved at lower pressures. Meanwhile, as the relative pressure became higher, H4 hysteresis loops were achieved which illustrated the evidence of the existence of a mesoporous surface. This is further confirmed in Fig. 7b, as indicated in the particle size distribution that equivalent particle sizes between the ranges of 18–42 nm were predominant and clustered on the surface of both the neat biochar and the magnetic biochar.

Optimization of dye adsorption using RSM

In this study, a second-order quadratic model was used to fit experimental data obtained from the adsorbed CV and SY on the synthesized OPF magnetic biochar using design expert 6.0.4. The result in terms of coded form is presented in Eqs. 15 and 16, respectively.

$$\begin{aligned} \%Y_1 = \text{CV Removal} = & 81.7 + 1.56 X_1 - 1.35X_2 \\ & - 2.78X_3 - 0.0897X_4 + 2.87X_1^2 - 0.08X_2^2 \\ & + 1.75X_3^2 + 4.75X_1X_2 + 1.01X_2X_3 \end{aligned} \quad (15)$$

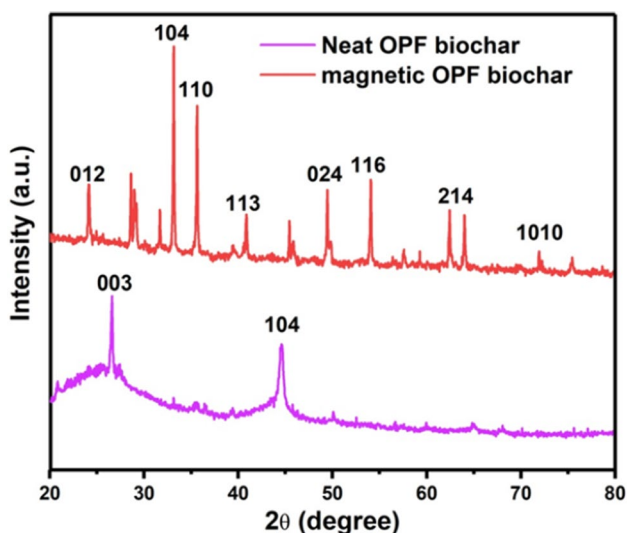


Fig. 6 X-ray diffraction (XRD) analysis of OPF biochar and magnetic biochar

Table 3 Specific surface area and pore structure variables of neat and magnetic OPF biochar

Samples	S _{BET} (m ² g ⁻¹)	Pore width (nm)	Pore volume (cm ³ g ⁻¹)
Neat OPF biochar	980.7854	1.9411	0.951918
Magnetic OPF biochar	162.1998	14.4705	1.173559

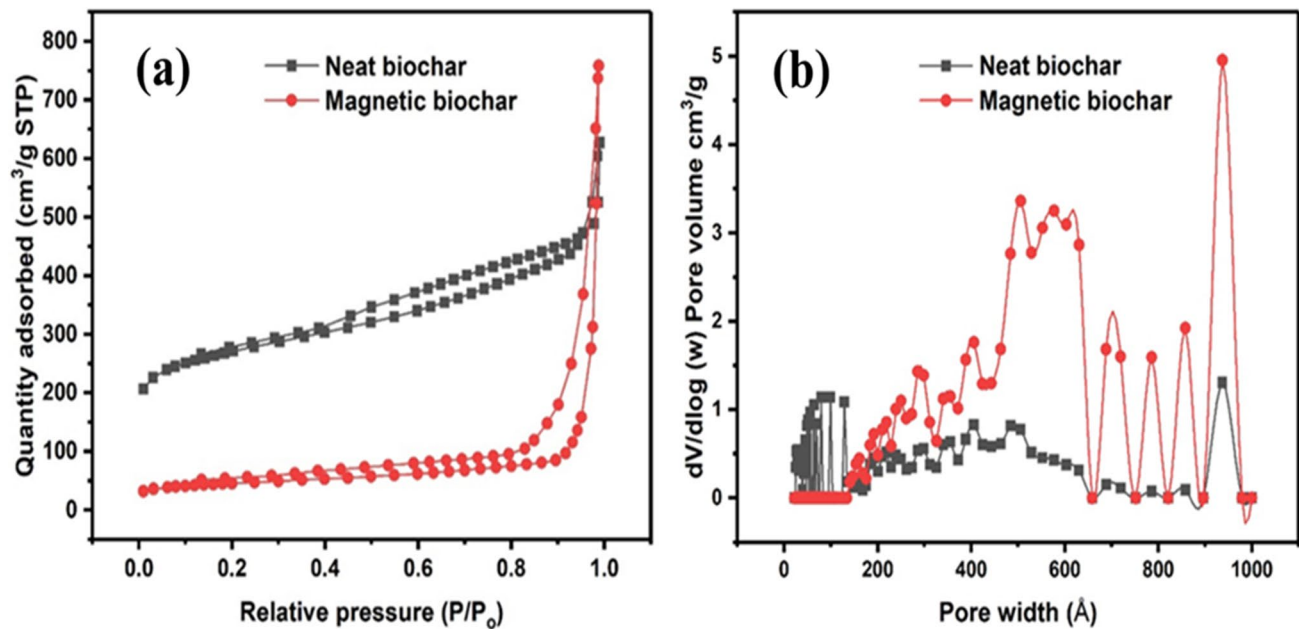


Fig. 7 Surface properties **a** N₂ adsorption/desorption isotherms for OPF biochar and magnetic biochar **b** Particle size distribution of neat biochar and magnetic biochar

$$\begin{aligned} \%Y_2 = \text{SY Removal} = & 79.58 + 2.72 X_1 - 1.37X_2 - 2.87X_3 \\ & - 1.54X_4 + 1.83X_1^2 - 0.59X_2^2 + 3.27X_3^2 + 1.23X_1X_3 \end{aligned} \quad (16)$$

The significance and adequacy of the quadratic models were evaluated using the result of ANOVA which analyses the variation between the significance of the model prediction and experimental error compared to the variation in terms of residual error. The positive/negative sign in the quadratic model equation reflects the synergistic and antagonistic effect of the process variables. It was clear that pH and adsorbent dose have a synergistic effect on CV removal efficiency and pH and initial concentration has a profound synergistic effect on the adsorption efficiency of SY which implies that enhanced adsorption efficiency of the magnetic biochar favours the increased adsorption of CV at low pH and increase in adsorption dose. Furthermore, an increase in adsorbent dosage and a low initial concentration increased the adsorption efficiency of magnetic biochar for the removal of CV dye molecules. Meanwhile, low pH and high initial concentration influenced improved adsorption of magnetic biochar for SY removal.

Statistical analysis

The Fisher's value F-test which expresses the ratio of the mean value and the residual error is used to evaluate this comparison (Motaghi et al. 2021). The result as presented in Table 4 and Table 5 revealed that the F-values for both responses

Table 4 ANOVA model for the second-order quadratic model for the adsorption of CV

Source	Sum of mean square	DF	Square value	F-value	P value
Model	18,132.96	14	1295.21	10.59	<0.0001
X ₁	13,950.95	1	13,950.95	114.03	<0.0001
X ₁ ²	2180.45	1	2180.45	17.82	0.0007
X ₃ ²	819.07	1	819.07	6.70	0.0206
X ₁ X ₂	217.42	1	217.42	1.78	0.0102
X ₂ X ₃	315.8	1	315.8	2.59	0.001

Table 5 ANOVA Model for the second-order quadratic model for the adsorption of SV

Source	Sum of mean square	DF	Square value	F-value	P value
Model	18,180.05	14	18,180.05	14.56	<0.0001
X ₁	12,027.46	1	12,027.46	134.85	<0.0001
X ₁ ²	3793.21	1	3793.21	42.53	<0.0001
X ₃ ²	712.82	1	712.82	7.99	0.0127
X ₁ X ₃	425.08	1	425.08	4.77	0.0453

demonstrated high values. As shown, it is revealed that model F-values for CV and SY removal were 10.59 and 14.56, respectively, at $P < 0.0001$, indicating the adequacy and significance of the model for the prediction of the responses can be

explained by the regression equation. The associated P value evaluates whether the *F*-values were large enough to indicate statistical significance (Dhiman et al. 2017; Wang et al. 2022). Both CV and SY adsorption models exhibit a type of Prob. > *F* (*P* values) less than 0.05 which indicated 95% confidence levels, thereby affirming that the proposed models are statistically significant under the designed operational conditions. For the adequacy of the fit model, the *R*² value must be greater than 0.80 including the difference between *R*² and *R*²_{Adj} which must be less than 0.20 (Rasuli et al. 2021; Liu et al. 2018).

As shown in Table 6, high correlation coefficient (*R*²) values of 0.9081 and 0.9315 for the OPF-derived magnetic biochar indicated the suitability of the model to estimate CV and SY removal, respectively. The effectiveness of the model was further demonstrated by the close agreement between the adjusted *R*² values (0.8223) and the predicted *R*² values (0.6138) for CV removal and the adjusted and predicted *R*² values 0.8675 and 0.7359, respectively, for SY removal. Adeq Precision' which is a measure of the signal-to-noise ratio is desirable if the value is greater than 4 (Wu et al. 2021b). The ratio of 12.79 and 15.59 indicated that the model exhibited adequate signal for CV and SY implying that the model can sufficiently navigate the design space. The magnitude of lack of fit proved to be insignificant for both CV and SY which corresponds to the lack of fit of *F*-values which was found at 0.72 and 0.54, respectively. Similarly, the lack of fit of *P* values was found at 0.69 (CV) and 0.81 (SY) indicating that the lack of fits was not significant relative to pure errors. Also, the *F*-values can be attributed to the noise levels in the model.

Interactive effect of the adsorption variables

Three-dimensional response surfaces represent CV and SY removal on the magnetic biochar. Each response surface plot was evaluated as a function of the interactive effect of two process variables. Figures 8a–c illustrated the 3D response surface plots for percentage removal of CV dye on magnetic biochar as a function of pH and adsorbent dose, pH and initial concentration, and adsorbent dosage and initial concentration, respectively. Accordingly, Fig. 8a shows that the response surface plot revealed that the removal percentage increased as pH increased from 7.5 to 11. At lower pH in the acidic condition, a decrease in the percentage removal of dye was achieved. In a basic medium, more hydroxide ions (OH⁻) are accumulated on the surface of the magnetic biochar which creates a negative surface charge of adsorbent thus favouring the adsorption

of positively charged CV through electrostatic interaction (Yamada et al. 2022). The increase in adsorbent dosage significantly improved the removal capacity, because of the availability of excess active sites for CV dye adsorption. Further increase in adsorbent dosage and removal capacity declines due to the agglomeration of adsorbent particles (Sabna et al. 2016). Figure 8b shows that significant removal of CV dye was found to be attributed to the good interactive influence of pH and initial concentration. An increase in pH as the initial concentration was decreased indicated that a lower initial concentration facilitates a larger sum of available adsorption sites on the sorbent surface which consequently increases the per cent removal of CV (Esmailian & O'Shea 2022). There was a slight increase but no significant difference in the per cent removal of CV (> 99%) as the adsorbent dosage was increased from 0.5 to 1 g/L at a lower initial concentration (Fig. 8c). Based on our results, it implies that a sorbent dose within 1 g/L at dye concentrations lower than 50 achieved optimum CV removal from the solution under controlled laboratory conditions. Figure 8d–f represents a 3D response surface plot as a function of the interaction of pH and adsorbent dosage, pH and initial concentration, and pH and temperature, respectively, for the removal of SY from the solution. It is revealed in Fig. 8d and e that the effect of the interaction of the process variables proportionately influenced the adsorption efficiency of the magnetic biochar for the removal of SY. High removal efficiency of magnetic biochar favoured the removal of SY at low pH (acidic medium) and low concentration. Similarly, an increase in adsorbent dosage favoured an increase in the per cent removal of SY at low concentrations indicating that sufficient adsorption sites were made available for the attachment of dye molecules on the surface of the magnetic biochar. An increase in temperature from 20 to 40 °C has no significant influence on the adsorption capacity of the biochar at a low concentration of the adsorbate (Fig. 8f).

The effect of the interaction of the independent variables on the responses is illustrated in Fig. 9(a and b) which shows that under optimum conditions of pH, adsorbent dose, initial concentration, and temperature at 95% confidence level (*P* < 0.05), the higher adsorption efficiency of magnetic biochar was achieved for the adsorption of CV and SY indicating that the adsorption of efficiency of the magnetic biochar was influenced optimally by the synergistic interaction of the four process variables.

Table 6 Summary of model fit for quadratic model data

Dyes	Std. dev	Mean	% CV	PRESS	<i>R</i> ²	Adj <i>R</i> ²	Pred <i>R</i> ²	Adeq precision	Lack of fit	
									<i>F</i> -value	<i>P</i> value
CV	11.06	70.16	15.76	7710.75	0.9081	0.8223	0.6138	12.79	0.72	0.691
SV	9.44	71.31	13.24	5154.63	0.9315	0.8675	0.7359	15.59	0.54	0.811

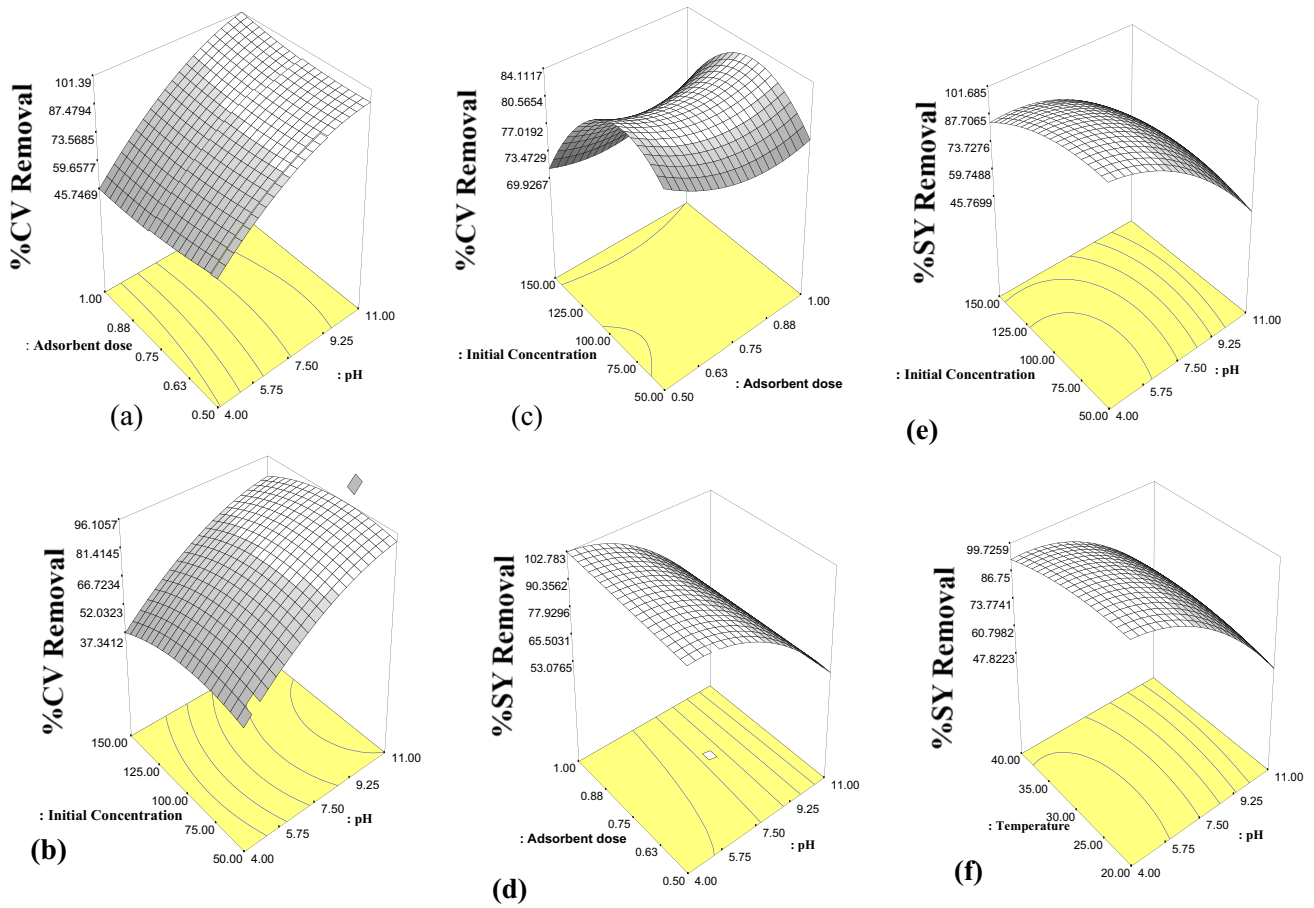
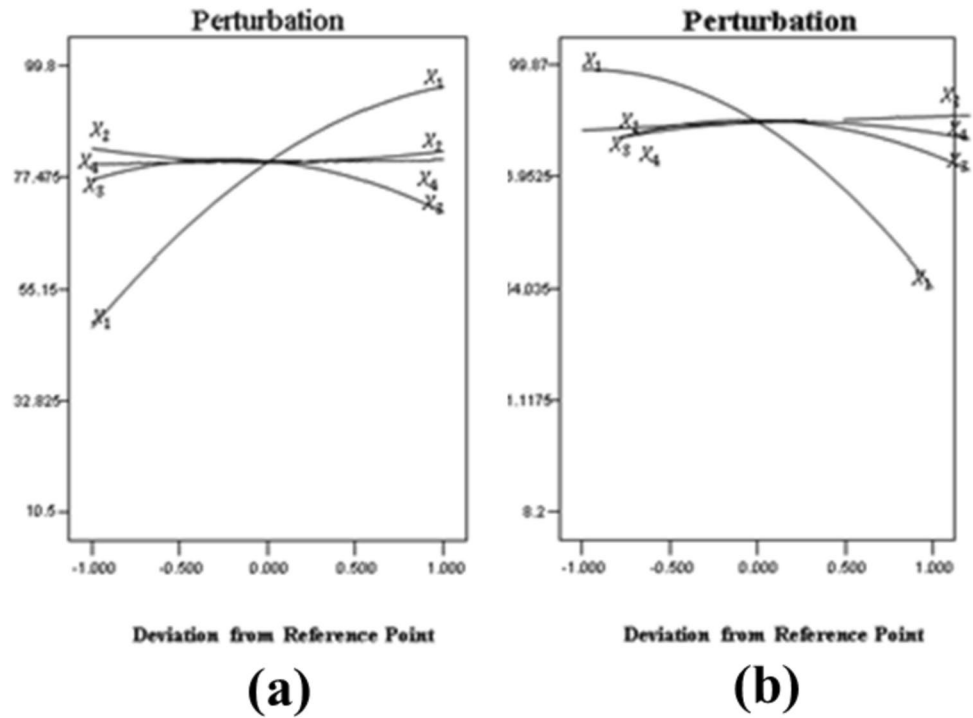


Fig. 8 3D Response surface plot of the interactive effect of factors for 9 a, b, c Adsorption of CV; 9 d, e and f Adsorption of SY

Fig. 9 Interaction of the four process variables for a Adsorption of CV and b Adsorption



Optimization of dye adsorption

The removal efficiency of the magnetic biochar can be rationalized by determining the best operational conditions of the process variables which enhanced the adsorption of CV and SY from the solution. This was achieved using the optimization function of the design expert. The optimum values of the parameters were obtained as a function of the desirability coefficient. The result is presented in Table 7. It was revealed that an increase in pH and adsorbent dosage at a low initial concentration favoured optimum adsorption efficiency of the magnetic biochar for CV removal. Conversely, in the case of SY removal, low pH and an increase in the adsorbent dosage at a low initial concentration significantly influenced the adsorption efficiency of the magnetic biochar. The highest per cent removal of CV was achieved at pH 11 ($P < 0.05$) in four-factor process variables. This means that under the highest basic condition, the optimum percentage removal of CV was achieved which implies that the dominance of negative charges on the surface of the magnetic biochar under alkaline conditions created the strong electrostatic attraction of the CV dye molecules to the surface of the biochar due to deprotonation of hydroxyl functional groups, most likely electrostatic attraction occurred between the positive charge of the dye molecules and the negative surface of the magnetic biochar (Al-Ghouti & Al-Absi 2020; Uddin et al. 2017). However, due to electrostatic repulsion as a result of the positively charged surface of the magnetic

biochar in an acidic medium, less adsorption occurs on the surface of the magnetic biochar. In contrast, increased per cent removal of SY corresponding to 100% was achieved ($P < 0.05$) on the surface of the magnetic biochar in an acidic medium (pH 4) and the adsorption capacity decreased in an alkaline state (Litefti et al. 2019). An increase in the initial concentration of the dyes from 50 to 150 mg/L resulted in to decrease in the adsorption capacity of the magnetic biochar. The optimum adsorption capacity of the adsorbent for the removal of CV and SV was favoured at low initial concentration and increased dosage. This behaviour can best be attributed to the availability of active adsorption sites which increases as the adsorbent mass increases.

Adsorption kinetics, isotherm, and thermodynamic studies

Adsorption kinetics

Kinetic study was investigated to understand the adsorption phenomenon of magnetic biochar for the removal of CV and SY. The adsorption kinetic data obtained according to Eqs. 3 and 4 were fitted to the pseudo-first-order (PFO) and pseudo-second-order (PSO). The linear relationship of the models is shown in Table 8. The linear plot of kinetic data expressing PFO and PSO is illustrated in Figs. 10a, b.

The results of the linear fit in terms of the high correlation coefficient of the kinetic models revealed that

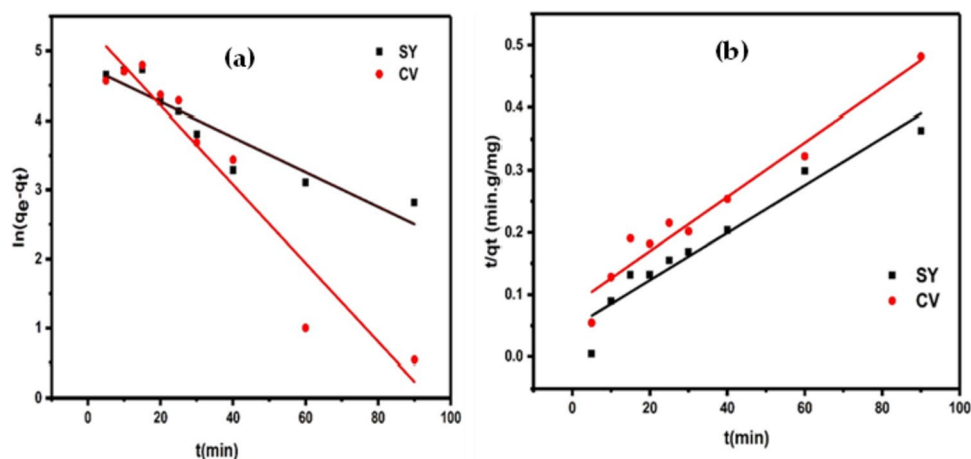
Table 7 Optimum operational conditions for dye adsorption

Variables	X_1	X_2	X_3	X_4	Desirability coefficient	Per cent removal	
						Actual value	Predicted value
CV	11	1	50	20	1	99.8	95.14
SV	4	1	50	20	1	99.87	100

Table 8 Kinetic model parameters for CV and SY dye removal

Kinetic model	Parameters	CV dye (mg/L)	SY dye (mg/L)
Pseudo-first order	$q_e, \text{exp (mg/g)}$	210.728	223.1
	$q_e, \text{cal (mg/g)}$	188.64	131.24
	$K_1 \text{ min}^{-1}$	0.0568	0.0298
	R^2	0.9116	0.9099
Pseudo-second order	$q_e, \text{exp (mg/g)}$	210.728	223.1
	$q_e, \text{cal (mg/g)}$	228.8	243.2
	$K_2(\text{g mg}^{-1} \text{ min.}^{-1})$	2.314×10^{-4}	6.17×10^{-4}
	R^2	0.9451	0.9501
Elovich	$\beta (\text{mg g}^{-1})$	0.0226	0.0241
	$\alpha (\text{mg g}^{-1} \text{ min}^{-1})$	32.94	28.87
	R^2	0.7473	0.8139
Intraparticle	$K_{id}(\text{mg g}^{-1} \text{ min}^{-1/2})$	17.977	16.5109
	C	31.564	72.565
	R^2	0.8133	0.8794

Fig. 10 Pseudo-first-order kinetics **a** adsorption of CV and SY; **b** Pseudo-second-order kinetics adsorption of CV and SY



PSO was found not to be only suitable for the adsorption process for both CV and SY but was also reflected in the equilibrium adsorption capacity of about 228.8 mg/g and 223.2 mg/g, respectively, relative to the result of the experimental adsorption capacities of CV (188.64 mg/g) and SY (221.3 mg/g). These results confirmed that the interaction of CV and SY molecules on the sites of the magnetic biochar followed the PSO model which at best can be described to be chemical in nature. The rate-limiting process may be influenced by the chemical interactions that involve the exchanging of valence forces or by the sharing electrons between magnetic biochar particles and the molecules of the dyes on the surface (Chen et al. 2019). Within the initial 15 min, the adsorption of CV increased rapidly with a removal efficiency of 30.9% achieved after which the rate of adsorption decreased until equilibrium was attained at 75 min of contact time with maximum adsorption efficiency of 85.7% achieved. For the adsorption of SY, adsorption was rapid in the initial 20 min of contact time with a removal efficiency of 63.29% achieved. After then, the rate of adsorption was slow until equilibrium was achieved after 90 min with a maximum removal efficiency of 93.02% achieved. Rapid adsorption of CV and SY at the initial stage of contact time can be attributed to the strong attraction between the dye molecules and the availability of large binding sites from the surface of the biochar. The diffusion of dye molecules drifts into the unoccupied adsorption sites slowly as the contact time increases until equilibrium is achieved after 75 and 90 min of CV and SY dye adsorption. Kumbhar et al. (2022) synthesized magnetic biochar composite from tea waste/ Fe_3O_4 for efficient adsorption of crystal violet dye. Their investigation achieved almost 98.7% adsorption of crystal violet dye at 90 min contact time.

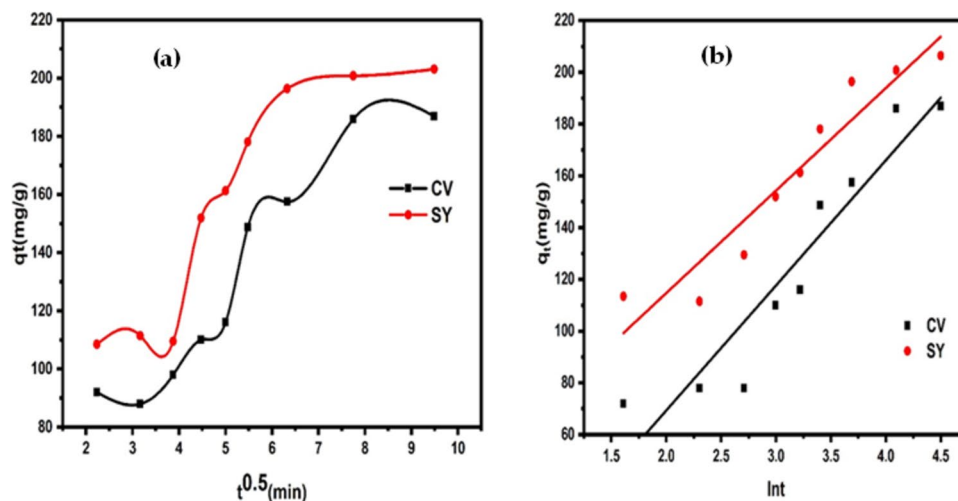
The contact time of adsorption on biochar for pollutant species in the wastewater treatment process depends on the scale, type of treatment system, and the targeted contaminant for remediation. For instance, in the study by Santhosh et al.

(2020) titled Synthesis and Characterization of Magnetic Biochar Adsorbents for the removal of Cr(VI) and Acid orange 7 dye from aqueous solution, maximum adsorption of 90 and 95% was achieved at the equilibrium time of 160 min for both pollutants. Oladipo et al. (2018) produced magnetic biochar from chicken bones which achieved 96% adsorption of Rhodamine B at a contact time of 60 min in a two-stage stirred adsorber system. Kumbhar et al. (2022) reported the synthesis of tea waste/ Fe_3O_4 magnetic composite (TWMC) for efficient adsorption of crystal violet dye: Isotherm, kinetic, and thermodynamic studies and achieved 98.7% adsorption of crystal violet dye at 90 min contact time.

It can be inferred that the adsorption of CV and SY on the surface of OPF-derived magnetic biochar was through a chemical reaction that occurred over a relatively long time of 75 and 90 min, respectively, before equilibrium adsorption was achieved for CV and SY adsorption.

To investigate the dynamics of the process of adsorption, intraparticle kinetic and Elovich models were applied according to Eqs. 5 and 6. As shown in Figs. 11a, b, it was revealed that the linear plots of CV and SY dye adsorption fitted to the intraparticle model indicated multi-linear plots. Accordingly, two substantial steps characterized the removal mechanism of both dyes. The first step signified the transfer of CV and SY dye molecules from the solution to the surface of the magnetic biochar otherwise influenced by instantaneous adsorption or adsorption on the external surface (Xu et al. 2021). The second step indicated pore diffusion of the dye molecules into the pores of the active sites of the magnetic biochar. Adsorption of dyes at this stage was predominantly by intraparticle diffusion. There seems to be a slowdown in intraparticle diffusion towards the end of the second stage due to low residual dye concentration in the dye solution (Choudhary et al. 2020). Other adsorption pathways other than only intraparticle diffusion defined the adsorption process of dye adsorption. It is clear that the kinetic data fitted to the intraparticle model revealed that

Fig. 11 **a** Intraparticle adsorption of CV and SY; **b** Elovich adsorption of CV and SY



the linearized plots did not pass through the origin for both CV and SY removal indicating that the adsorption rate was controlled by the external surface adsorption and liquid film diffusion (Fan et al. 2017).

The Elovich model which is the fourth kinetic model used defines expresses heterogeneous surface compatible with chemisorption kinetics (Rahpeima et al. 2018). The R^2 value from the model which were 0.747 and 0.814 for CV and SV removal indicates that the irregular microstructure of the magnetic biochar partly may have influenced the adsorption process.

Adsorption isotherm

The equilibrium adsorption models which were Langmuir, Freundlich, Temkin, and Dubinin–Radushkevich (D-R) isotherm models were used to fit experimental data to describe the adsorption process of CV and SY on the magnetic biochar according to Eq. 7–10. The results from the linearized plots revealed that the Langmuir model exhibited the highest R^2 value of 0.991 and 0.98 for the removal of CV and SY, respectively, which indicated the adsorption process occurred on the monolayer surface of the magnetic biochar (Fig. 12a). The high maximum adsorption capacity (q_{max}) and K_L values for both dyes (Table 9) confirmed that Langmuir's theory can effectively explain the removal of the dyes on the surface of the magnetic biochar. The values of the dimensionless constant R_L from the expression of $R_L = \frac{1}{1+C_0K_L}$ for CV and SY removal were 0.00011 and 0.00009 which indicated favourable adsorption of the dyes on the magnetic biochar since $0 < R_L < 1$ describes favourable adsorption, $R_L > 1$ indicates unfavourable adsorption, $R_L = 0$ implies irreversible adsorption, and $R_L = 1$ demonstrates linear

adsorption (Oyekanmi et al. 2021; Chen et al. 2020). The order of the values of R_L which showed that $CV > SY$ indicated consistency with the order of the values of the maximum adsorption capacities of the two dyes which were 149.03 and 342.47 mg/g, respectively, demonstrating that the adsorption process was significant on a monolayer coverage on the magnetic biochar.

As shown in Table 10, multilayer adsorption of CV and SV on the heterogeneous surface of the magnetic biochar as represented by the model Eq. (8) described the experimental data fitted to the Freundlich isotherm. The slope of $1/n$ and the intercept which was obtained from $\ln K_f$ the linearized plot revealed that occasionally the removal of the dyes occurred on the surface of the magnetic biochar as a result of unequal sites for adsorption on layers of the adsorbent surface (Fig. 12b). The R^2 values of 0.9730 and 0.9599 were achieved for the adsorption of CV and SY, respectively.

Temkin isotherm assumed that the heat of adsorption of dye molecules decreased linearly with increased adsorption coverage due to adsorbent–adsorbate interaction. The slope B and intercept $\ln C_f$ obtained from the isotherm Eq. (6) were evaluated from the linearized plot as shown in Table 5. This is illustrated in Fig. 13c. The R^2 values of CV and SY on the magnetic biochar were 0.9759 and 0.9780, respectively.

The Dubinin–Radushkevich (D-R) isotherm which describes the mechanism of dye adsorption and the energy of adsorption on the magnetic biochar was evaluated according to Eq. (10). The slope K_{ad} and the intercept q_s obtained from the linearized plots are shown in Table 5 including the adsorption energy equation (E) expressed K_j/mol as indicated in Fig. 13d. It was revealed that the correlation coefficients were lower than fitted data to other investigated isotherm equations. The nature of the adsorption process is determined by the magnitude of the adsorption energy equation. The nature of the adsorption process

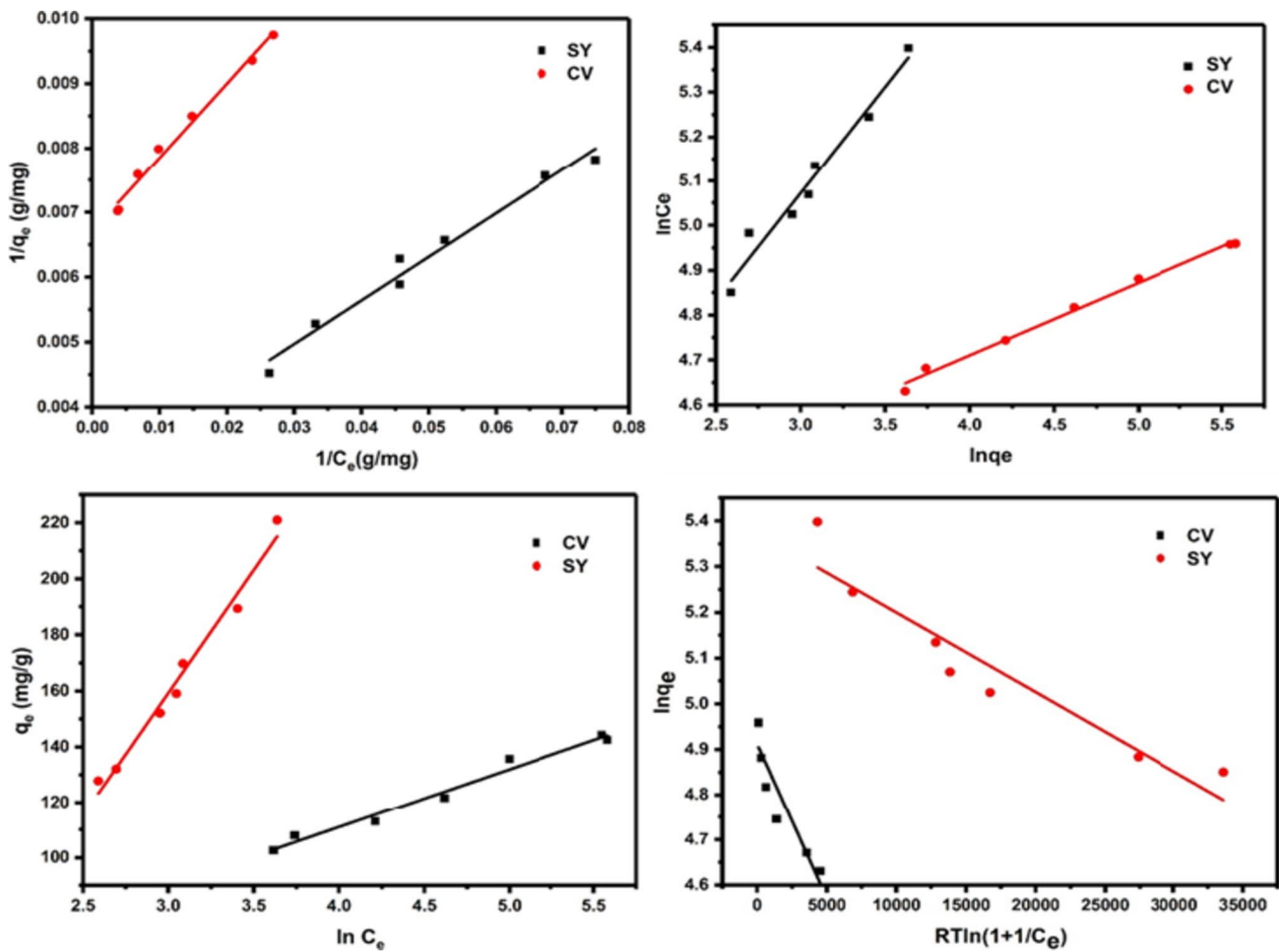


Fig. 12 Equilibrium isotherms Adsorption of CV and SY; a Langmuir; b Freundlich c Temkin; d D-R

Table 9 Isotherm model parameters for CV and SY dye removal

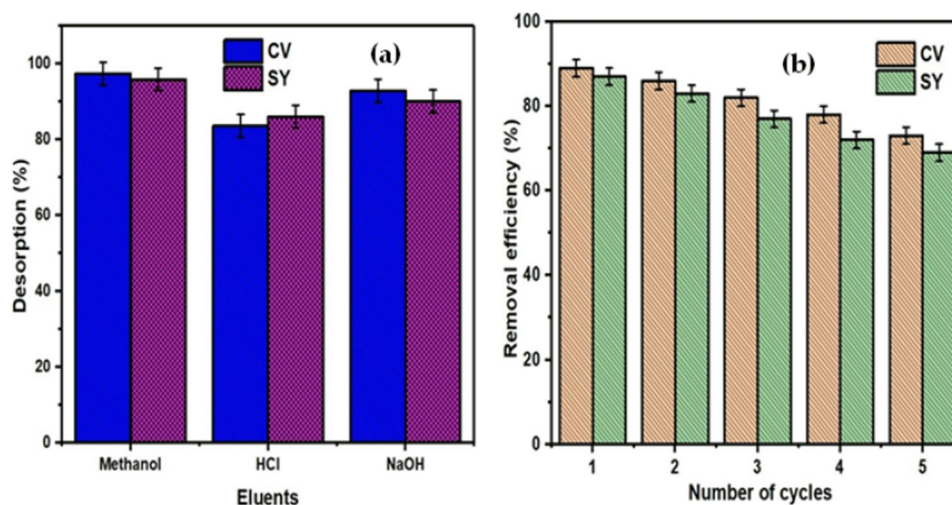
Isotherm model	Parameters	CV Dye (mg/L)	SY Dye (mg/L)
Langmuir	q_{max} (mg g ⁻¹)	149.03	342.47
	R_L	1×10^{-4}	9.01×10^{-5}
	R^2	0.9864	0.9816
Freundlich	K_f (L. mg ⁻¹)	55.98	38.08
	n	5.9382	2.094
	R^2	0.9730	0.9595
Temkin	a_T (L. g - 1)	3.6536	0.3061
	B	20.96	87.744
	R^2	0.9759	0.9781
Dubinin–Radushkevich	q_s (mg g ⁻¹)	15.9156	21.565
	K_{ad}	6.8×10^{-5}	1.739×10^{-5}
	E	85.262	169.55
	R^2	0.8342	0.8845

Table 10 The thermodynamic parameters for the adsorption of CV and SY on magnetic biochar

Temp (K)	ΔG (kJ/mol)	ΔH (kJ/mol)	ΔS (J/mol/K)
CV			
293 K	-3.226	1.92	0.01758
298 K	-3.325		
303 K	-3.402		
SY			
293 K	-1.878	0.725	0.00889
298 K	-1.923		
303 K	-1.967		

is determined by the magnitude of the adsorption energy equation which implies that adsorption is by physisorption process if ($2 < E < 8$ kJ/mol) but the adsorption is defined by the chemisorption process if ($8 < E < 16$ kJ/mol). The mean free energy as evaluated from the D-R model indicated that the magnitude of E value was 85.26 and 168.55 for CV and SY, respectively, which affirmed that the adsorption of both

Fig. 13 **a** Desorption **b** regeneration efficiency of magnetic biochar for CV and SY removal



dyes on the surface of the magnetic biochar was by chemisorption process.

Thermodynamic study

To better understand the feasibility of magnetic biochar and its thermodynamic behaviour to describe the nature of the adsorption process of CV and SY molecules on its surface, the thermodynamic parameters were evaluated from equilibrium constants.

From the linearized plot of Van't Hoff equation ($\ln K_d$ against $1/T$), ΔH° and ΔS° could be evaluated from the slope, and ΔS° is calculated from the intercept, respectively. The results are presented in Table 10. The positive values of ΔH° (change of enthalpy) indicated that the adsorption process was endothermic in nature for both CV and SY removal. Furthermore, the state of disorderliness and spontaneity at the interface of the magnetic biochar and dye molecules as expressed by the positive values of change of entropy ΔS° evidently described the adsorption process of CV and SY. It reflected the release of energy during the transfer of the dye molecules from the aqueous phase to the solid phase (Gharbani & Mehrizad 2022). Furthermore, the negative values obtained from the Gibbs free energy confirmed that the adsorption of CV and SY on magnetic biochar was spontaneous at all the studied temperatures.

Regeneration of adsorbent

The economic feasibility of adsorbent depends on its recyclability and desorption potential. In this study, 0.2 mol/L of methanol, HCl, and NaOH were applied, respectively, as desorption solution for the recovery of CV and SY from the dye-saturated magnetic biochar. It was revealed that the desorption efficiency of the magnetic biochar partly increased using the three eluting agents in the order of

methanol > NaOH > HCl (Fig. 13a). Optimum desorption efficiency greater than 99% recovery of CV and SY was achieved using methanol as eluent. Therefore, the regeneration potential of the magnetic biochar was examined after each successive adsorption–desorption cycle. The adsorbent was considered fully regenerated after the dyes had been completely desorbed. It is shown in Fig. 13b that a slight decrease without significant difference in the adsorption efficiency of the magnetic biochar was achieved for CV (89.4%) and SY (87.2%) removal in the first cycle of the adsorption study. There was no significant change in the adsorption capacity until the 5th cycle indicating that the adsorption capacity of the magnetic biochar was not reduced relative to the freshly used samples which indicates its high regeneration capacity. Therefore, it can be inferred that methanol can effectively regenerate the adsorbents after the desorption of CV and SY dyes from spent magnetic biochar. The intrinsic property and the remarkable reusability potential showed that OPF-derived magnetic biochar is economically viable and can be utilized as a promising bio-adsorbent in wastewater treatment.

Possible adsorption mechanism

The underlying interactive mechanism is significant for the recovery of dye molecules by applying different adsorbents. Due to unique structural properties and active functional groups, magnetic biochar can interact with different dye molecules via different adsorption mechanisms. The evaluation of adsorption mechanisms enables the design and modification of surfaces of adsorbents to enhance interaction, and diffusion pathways of dye molecules and subsequently to enhance adsorption capacity. The selectivity of removal of dye molecules on the adsorbent–adsorbate interface creates effective design and fabrication of selective adsorbents. This

section creates an insight into possible interaction mechanisms for the adsorption of CV and SY on the surface of magnetic biochar.

OPF-derived magnetic biochar mainly comprises cellulose, hemicellulose, and lignin which has oxygen-containing functional groups such as hydroxyl (OH) and carboxylic (-COOH) groups present in abundance on the surface. The possible adsorption mechanism of biochar surface with dye molecules is represented in Fig. 14. In acidic medium pH, the biochar surface was favourable for the removal of anionic dye (Sunset yellow) because the surface charge of biochar was predominated by a positive charge due to the presence of more H⁺. In this case, anionic dye molecules bind with positively charged biochar surfaces due to electrostatic interaction (Goswami et al. 2022; Inyang et al. 2016; Li et al. 2022).

Biochar-COOH + H⁺..... Biochar-COOH₂⁺ (In acidic condition).

Biochar-OH + H⁺..... Biochar-OH₂⁺ (In acidic condition).

On the other hand, in basic pH, the biochar surface is favourable for the removal of cationic dye (Crystal violet) because the surface charge of biochar is negatively charged due to the presence of more OH⁻. In this case, cationic dye molecules bind with negatively charged biochar surface with electrostatic interaction (Ma et al. 2020; Wu et al. 2021a).

Biochar-COOH Biochar-COO⁻ (In basic condition).

Biochar-OH Biochar-O⁻ (In basic condition).

Conclusion

The physicochemical properties of magnetic biochar produced from OPF via the facile synthesis co-precipitation method proved to possess effective adsorption capacity for the removal of CV and SY dyes from aqueous solution. The saturation magnetization of OPF biochar was found to be 8.41 emu/g, coercivity (Hc) of 83.106 G, and retentivity (Mr) of 1.475 emu/g which implies that OPF magnetic biochar can be facily separated from aqueous solution. The result also demonstrated superparamagnetic properties provided suitable magnetic responsive characteristics to an external magnetic field. The influence of operational parameters of pH, adsorbent dosage, the initial concentration, and temperature investigated using the CCD of the RSM optimally enhanced the adsorption capacity of the magnetic biochar as reflected in its high removal efficiency for CV and SY removal. Kinetics of adsorption showed that the pseudo-second-order model best-fitted equilibrium data implying that the adsorption process of both dye molecules was predominated by chemisorption. The isotherm experimental data were fitted best to the Langmuir isotherm model which demonstrated that the removal of CV and SY dyes on the magnetic biochar occurred on monolayer surface coverage. Maximum adsorption capacities of CV and SY dyes (149.03 and 342.47 mg/g), respectively, indicated that the adsorption process was significantly on a monolayer coverage on the magnetic biochar.

Furthermore, the adsorption process was predominantly spontaneous and endothermic in nature. The regeneration

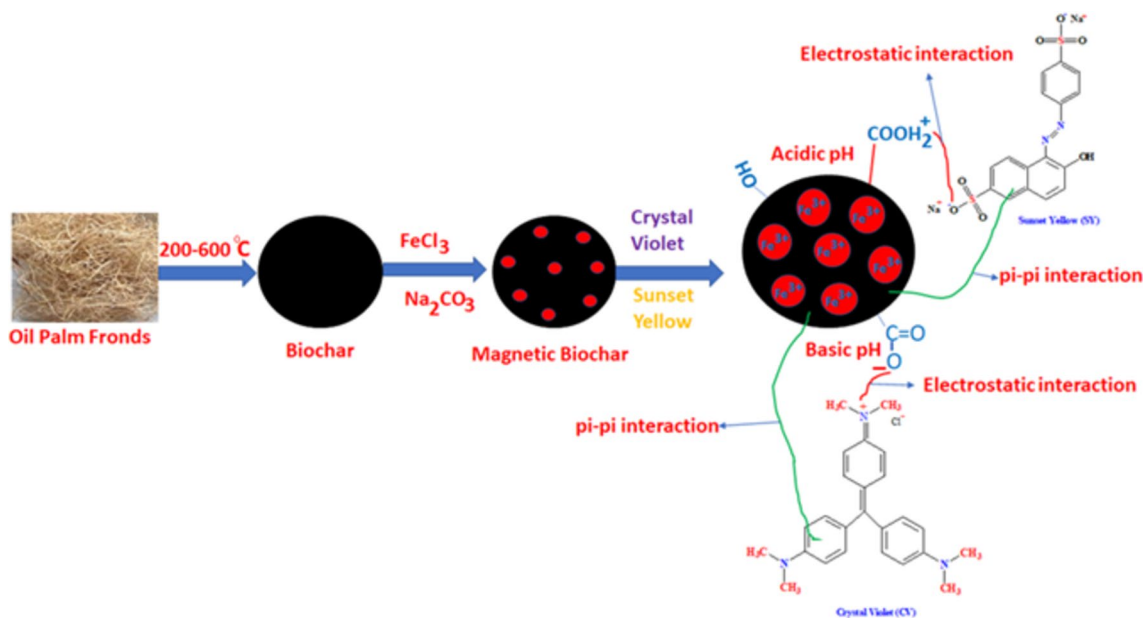


Fig. 14 Possible adsorption mechanism of dye adsorption on magnetic biochar

potential of the spent magnetic biochar indicated that desorption of the dye molecules and its adsorption capacity was not largely affected after 5 cycles of regeneration relative to adsorption on freshly synthesized magnetic biochar. The adsorption capacity of the OPF-derived magnetic biochar for the adsorption of CV and SY from aqueous solution was attributed to the adsorbent–adsorbate interaction which was achieved by electrostatic attraction. The surface properties demonstrated that OPF magnetic biochar can be effectively utilized for the treatment of dyes containing effluent.

Supplementary Information The online version contains supplementary material available at <https://doi.org/10.1007/s13201-023-02060-8>.

Acknowledgements This work was supported by Tenaga Nasional Berhad (TNB) and UNITEN through the BOLD Refresh Postdoctoral Fellowships under the project code of J510050002-IC-6 BOLDREFRESH2025-Centre of Excellence.

Funding This work was funded by the Universiti Tenaga Malaysia, Kajang, Malaysia under PRGS with grant 20200102PRGS.

Declarations

Conflict of interest The authors declare that they have no conflict of interest.

Ethical approval Not applicable.

Open Access This article is licensed under a Creative Commons Attribution 4.0 International License, which permits use, sharing, adaptation, distribution and reproduction in any medium or format, as long as you give appropriate credit to the original author(s) and the source, provide a link to the Creative Commons licence, and indicate if changes were made. The images or other third party material in this article are included in the article's Creative Commons licence, unless indicated otherwise in a credit line to the material. If material is not included in the article's Creative Commons licence and your intended use is not permitted by statutory regulation or exceeds the permitted use, you will need to obtain permission directly from the copyright holder. To view a copy of this licence, visit <http://creativecommons.org/licenses/by/4.0/>.

References

- Ahmad, R., Ansari, K. 2022. Fabrication of alginate@ silver nanoparticles (Alg@ AgNPs) bionanocomposite for the sequestration of crystal violet dye from aqueous solution. *Int J Biol Macromol*
- Ahmadipouya S, Mousavi SA, Shokrgozar A, Mousavi DV (2022) Improving dye removal and antifouling performance of polysulfone nanofiltration membranes by incorporation of UiO-66 metal-organic framework. *J Environ Chem Eng* 10(3):107535
- Akgül G, Maden TB, Diaz E, Jiménez EM (2019) Modification of tea biochar with Mg, Fe, Mn and Al salts for efficient sorption of PO4³⁻ and Cd²⁺ from aqueous solutions. *J Water Reuse Desalination* 9(1):57–66
- Al-Ghouti MA, Al-Absi RS (2020) Mechanistic understanding of the adsorption and thermodynamic aspects of cationic methylene blue dye onto cellulosic olive stones biomass from wastewater. *Sci Rep* 10(1):15928
- Arafat Hossain M, Ganesan P, Jewaratnam J, Chinna K (2017) Optimization of process parameters for microwave pyrolysis of oil palm fiber (OPF) for hydrogen and biochar production. *Energy Convers Manage* 133:349–362
- Chen S, Qin C, Wang T, Chen F, Li X, Hou H, Zhou M (2019) Study on the adsorption of dyestuffs with different properties by sludge-rice husk biochar: adsorption capacity, isotherm, kinetic, thermodynamics and mechanism. *J Mol Liq* 285:62–74
- Chen D, Wang Q, Li Y, Li Y, Zhou H, Fan Y (2020) A general linear free energy relationship for predicting partition coefficients of neutral organic compounds. *Chemosphere* 247:125869
- Choudhary M, Kumar R, Neogi S (2020) Activated biochar derived from *Opuntia ficus-indica* for the efficient adsorption of malachite green dye, Cu²⁺ and Ni²⁺ from water. *J Hazard Mater* 392:122441
- Dhiman N, Shukla S, Kisku G (2017) Statistical optimization of process parameters for removal of dyes from wastewater on chitosan cenospheres nanocomposite using response surface methodology. *J Clean Prod* 149:597–606
- Dong Y, Yuan H, Ge D, Zhu N (2022) A novel conditioning approach for amelioration of sludge dewaterability using activated carbon strengthening electrochemical oxidation and realized mechanism. *Water Res* 220(March):118704
- Eltaweil AS, Ali Mohamed H, Abd El-Monaem EM, El-Subruiti GM (2020) Mesoporous magnetic biochar composite for enhanced adsorption of malachite green dye: characterization, adsorption kinetics, thermodynamics and isotherms. *Adv Powder Technol* 31(3):1253–1263
- Esmailian A, O'Shea KE (2022) Application of dimensional analysis in sorption modeling of the styryl pyridinium cationic dyes on reusable iron based humic acid coated magnetic nanoparticles. *Chemosphere* 286:131699
- Fan S, Wang Y, Wang Z, Tang J, Li X (2017) Removal of methylene blue from aqueous solution by sewage sludge-derived biochar: Adsorption kinetics, equilibrium, thermodynamics and mechanism. *J Environ Chem Eng* 5(1):601–611
- Harith Zafrul Fazry, A., Sapawe, N., Izhar Fahimi Abdul Aziz, A., Zafri Haiqal Zainudin, M., Hakimi Haizal Hafiz, M., Aiman Farhan Idris, M., Farhan Hanafi, M., Farhan Mohd Fozi, M. 2018. Microwave induced HNO₂ and H₃PO₄ activation of oil palm frond (OPF) for removal of malachite green. *Mater Today: Proc* 5:22143–22147.
- Feng C, Huang M, Huang C-P (2023) Specific chemical adsorption of selected divalent heavy metal ions onto hydrous γ -Fe₂O₃-biochar from dilute aqueous solutions with pH as a master variable. *Chem Eng J* 451:138921
- Frankel ML, Bhuiyan TI, Veksha A, Demeter MA, Layzell DB, Helleur RJ, Hill JM, Turner RJ (2016) Removal and biodegradation of naphthenic acids by biochar and attached environmental biofilms in the presence of co-contaminating metals. *Biores Technol* 216:352–361
- Gharbani P, Mehrizad A (2022) Preparation and characterization of graphitic carbon nitrides/polyvinylidene fluoride adsorptive membrane modified with chitosan for Rhodamine B dye removal from water: Adsorption isotherms, kinetics and thermodynamics. *Carbohydr Polym* 277:118860
- Goswami L, Kushwaha A, Kafle SR, Kim B-S (2022) Surface modification of biochar for dye removal from wastewater. *Catalysts* 12(8):817
- Haghdoust S, Arabkhani P, Ghaderi S, Ghaedi M, Asfaram A (2023) Rapid microwave-assisted synthesis of a magnetic biochar@ ZIF-67: an efficient nanocomposite-based adsorbent for the dye-contaminated water cleanup. *New J Chem* 47(19):9257–9270
- Hu J, Zhao L, Luo J, Gong H, Zhu N (2022) A sustainable reuse strategy of converting waste activated sludge into biochar for contaminants removal from water: modifications, applications and perspectives. *J Hazard Mater* 438:129437

- Inyang MI, Gao B, Yao Y, Xue Y, Zimmerman A, Mosa A, Pullamanappallil P, Ok YS, Cao X (2016) A review of biochar as a low-cost adsorbent for aqueous heavy metal removal. *Crit Rev Environ Sci Technol* 46(4):406–433
- Isgiyarta J, Sudarmanta B, Prakoso JA, Jannah EN, Saleh AR (2022) Micro-grid oil palm plantation waste gasification power plant in Indonesia: techno-economic and socio-environmental analysis. *Energies* 15(5):1782
- Jasri K, Abdulhameed AS, Jawad AH, Allothman ZA, Yousef TA, Al Duaij OK (2023) Mesoporous activated carbon produced from mixed wastes of oil palm frond and palm kernel shell using microwave radiation-assisted K_2CO_3 activation for methylene blue dye removal: optimization by response surface methodology. *Diam Relat Mater* 131:109581
- Jie Y, Yuanyuan Li, Yi S, Huawei T, Jitong Z (2023) Effect of magnesium ions on the mechanical properties of soil reinforced by microbially induced carbonate precipitation. *J Mater Civ Eng* 35(11):4023413
- Jung K-W, Choi BH, Jeong T-U, Ahn K-H (2016) Facile synthesis of magnetic biochar/Fe₃O₄ nanocomposites using electro-magnetization technique and its application on the removal of acid orange 7 from aqueous media. *Biores Technol* 220:672–676
- Kamali N, Rashidi Mehrabadi A, Mirabi M, Zahed MA (2021) Comparison of micro and nano MgO-functionalized vinasse biochar in phosphate removal: micro-nano particle development, RSM optimization, and potential fertilizer. *J Water Proc Eng* 39:101741
- Katibi KK, Yunos KF, Che Man H, Aris AZ, bin Mohd Nor, M.Z., binti Azis, R.S. (2021) Recent advances in the rejection of endocrine-disrupting compounds from water using membrane and membrane bioreactor technologies: a review. *Polymers* 13(3):392
- Khan ZH, Gao M, Qiu W, Qaswar M, Islam MS, Song Z (2020) The sorbed mechanisms of engineering magnetic biochar composites on arsenic in aqueous solution. *Environ Sci Pollut Res* 27(33):41361–41371
- Khatun R, Reza MIH, Moniruzzaman M, Yaakob Z (2017) Sustainable oil palm industry: the possibilities. *Renew Sustain Energy Rev* 76:608–619
- Kong L, Liu G (2021) Synchrotron-based infrared microspectroscopy under high pressure: an introduction. *Matter Radiat Extremes* 6(6)
- Kumar V (2019) Adsorption kinetics and isotherms for the removal of rhodamine B dye and Pb²⁺ ions from aqueous solutions by a hybrid ion-exchanger. *Arab J Chem* 12(3):316–329
- Kumbhar P, Narale D, Bhosale R, Jambhale C, Kim J-H, Kolekar S (2022) Synthesis of tea waste/Fe₃O₄ magnetic composite (TWMC) for efficient adsorption of crystal violet dye: isotherm, kinetic and thermodynamic studies. *J Environ Chem Eng* 10(3):107893
- Li M, Wei D, Liu T, Liu Y, Yan L, Wei Q, Du B, Xu W (2019) EDTA functionalized magnetic biochar for Pb(II) removal: Adsorption performance, mechanism and SVM model prediction. *Sep Purif Technol* 227:115696
- Li X, Xu J, Luo X, Shi J (2022) Efficient adsorption of dyes from aqueous solution using a novel functionalized magnetic biochar: synthesis, kinetics, isotherms, adsorption mechanism, and reusability. *Biores Technol* 360:127526
- Litefti K, Freire MS, Stitou M, González-Álvarez J (2019) Adsorption of an anionic dye (Congo red) from aqueous solutions by pine bark. *Sci Rep* 9(1):16530
- Liu W, Zheng J, Ou X, Liu X, Song Y, Tian C, Rong W, Shi Z, Dang Z, Lin Z (2018) Effective extraction of Cr(VI) from hazardous gypsum sludge via controlling the phase transformation and chromium species. *Environ Sci Technol* 52(22):13336–13342
- Ma J, Zhou B, Zhang H, Zhang W (2020) Fe/S modified sludge-based biochar for tetracycline removal from water. *Powder Technol* 364:889–900
- Meng X, Scheidemantle B, Li M, Wang Y-Y, Zhao X, Toro-González M, Singh P, Pu Y, Wyman CE, Ozcan S, Cai CM, Ragauskas AJ (2020) Synthesis, characterization, and utilization of a lignin-based adsorbent for effective removal of Azo dye from aqueous solution. *ACS Omega* 5(6):2865–2877
- Mittal H, Al Alili A, Morajkar PP, Alhassan SM (2021) Graphene oxide crosslinked hydrogel nanocomposites of xanthan gum for the adsorption of crystal violet dye. *J Mol Liq* 323:115034
- Molla A, Li Y, Mandal B, Kang SG, Hur SH, Chung JS (2019) Selective adsorption of organic dyes on graphene oxide: Theoretical and experimental analysis. *Appl Surf Sci* 464:170–177
- Motaghi, H., Arabkhani, P., Parvinnia, M., Asfaram, A. 2021. Simultaneous adsorption of cobalt ions, azo dye, and imidacloprid pesticide on the magnetic chitosan/activated carbon@ UiO-66 bio-nanocomposite: optimization, mechanisms, regeneration, and application. *Separat Purification Technol* p 120258
- Nizam NUM, Hanafiah MM, Mahmoudi E, Mohammad AW, Oye-kanmi AA (2022) Effective adsorptive removal of dyes and heavy metal using graphene oxide based Pre-treated with NaOH/H₂SO₄ rubber seed shells synthetic graphite Precursor: equilibrium Isotherm, kinetics and thermodynamic studies. *Sep Purif Technol* 289:120730
- Nordin NA, Sulaiman O, Hashim R, Kassim MH, Mohamad. (2017) Oil palm frond waste for the production of cellulose nanocrystals. *J Phys Sci* 28(2):115–126
- Oladipo AA, Ifebajo AO (2018) Highly efficient magnetic chicken bone biochar for removal of tetracycline and fluorescent dye from wastewater: Two-stage adsorber analysis. *J Environ Manage* 209:9–16
- Othmani A, John J, Rajendran H, Mansouri A, Sillanpää M, Velayudhaperumal Chellam P (2021) Biochar and activated carbon derivatives of lignocellulosic fibers towards adsorptive removal of pollutants from aqueous systems: Critical study and future insight. *Sep Purif Technol* 274:119062
- Oye-kanmi AA, Ahmad A, Hossain K, Rafatullah M (2019) Statistical optimization for adsorption of Rhodamine B dye from aqueous solutions. *J Mol Liq* 281:48–58
- Oye-kanmi AA, Ahmad A, Mohd Setapar SH, Alshammari MB, Jawaid M, Hanafiah MM, Abdul Khalil HPS, Vaseashta A (2021) Sustainable durio zibethinus-derived biosorbents for congo red removal from aqueous solution: statistical optimization. *Isotherms Mech Stud Sustain* 13(23):13264
- Oye-kanmi AA, Hanafiah MM, Dele-Afolabi TT, Ahmad A, Alshammari MB (2022) Development of nanoparticles loaded composites from agricultural wastes for cationic dye removal from aqueous solution – A review. *J Environ Chem Eng* 10(5):108263
- Rahpeima S, Javanbakht V, Esmaili J (2018) Synthesis and characterization of activated carbon/maghemite/starch magnetic bionanocomposite and its application for permanganate removal from aqueous solution. *J Inorg Organomet Polym Mater* 28(1):195–211
- Rasuli L, Dehghani MH, Alimohammadi M, Yaghmaeian K, Rastkari N, Salari M (2021) Mesoporous metal organic frameworks functionalized with the amino acids as advanced sorbents for the removal of bacterial endotoxins from water: Optimization, regression and kinetic models. *J Mol Liq* 339:116801
- Rizal S, HPS AK, Oye-kanmi AA, Gideon ON, Abdullah CK, Yahya EB, Rahman AA (2021) Cotton wastes functionalized biomaterials from micro to nano: a cleaner approach for a sustainable environmental application. *Polymers* 13(7):1006
- Rubangakene NO, Elkady M, Elwardany A, Fujii M, Sekiguchi H, Shokry H (2023) Effective decontamination of methylene blue from aqueous solutions using novel nano-magnetic biochar from green pea peels. *Environ Res* 220:115272
- Sabna V, Thampi SG, Chandrakaran S (2016) Adsorption of crystal violet onto functionalised multi-walled carbon nanotubes: equilibrium and kinetic studies. *Ecotoxicol Environ Saf* 134:390–397

- Saeed AH, A., Yub Harun, N., Mahmoud Nasef, M., Al-Fakih, A., Abdulhakim Saeed Ghaleb, A., Kolawole Afolabi, H. (2022) Removal of cadmium from aqueous solution by optimized rice husk biochar using response surface methodology. *Ain Shams Eng J* 13(1):101516
- Saeki D, Yonamine G, Matsuyama H (2021) Effect of hydrophilic polymer modification of reverse osmosis membrane surfaces on organic adsorption and biofouling behavior. *Coll Surf, A* 609:125680
- Santhosh C, Daneshvar E, Tripathi KM, Baltrėnas P, Kim T, Baltrėnaitė E, Bhatnagar A (2020) Synthesis and characterization of magnetic biochar adsorbents for the removal of Cr (VI) and Acid orange 7 dye from aqueous solution. *Environ Sci Pollut Res* 27:32874–32887
- Shitu IG, Talib ZA, Chi JL, Ying K, Awang MM, Baqiah H (2020) Influence of tartaric acid concentration on structural and optical properties of CuSe nanoparticles synthesized via microwave assisted method. *Res Phys* 17(March):103041
- Shitu IG, Katibi KK, Taura LS, Muhammad A, Chikomawa IM, Adamu SB, Iya D, Garba S (2023) X-ray diffraction (XRD) profile analysis and optical properties of Klockmannite copper selenide nanoparticles synthesized via microwave assisted technique. *Ceram Int* 49(8):12309–12326
- Siddiqui AJ, Kumari N, Adnan M, Kumar S, Abdelgadir A, Saxena J, Badraoui R, Snoussi M, Khare P, Singh R (2023) Impregnation of modified magnetic nanoparticles on low-cost agro-waste-derived biochar for enhanced removal of pharmaceutically active compounds: performance evaluation and optimization using response surface methodology. *Water* 15(9):1688
- Singh P, Sulaiman O, Hashim R, Peng LC, Singh RP (2013) Using biomass residues from oil palm industry as a raw material for pulp and paper industry: potential benefits and threat to the environment. *Environ Dev Sustain* 15:367–383
- Sun X, Fu H, Bao M, Liu W, Luo C, Li Y, Li Y, Lu J (2022) Development of a new hydrophobic magnetic biochar for removing oil spills on the water surface. *Biochar* 4(1):60
- Thasneema K, Dipin T, Thayyil MS, Sahu PK, Messali M, Rosalin T, Elyas K, Saharuba P, Anjitha T, Hadda TB (2021) Removal of toxic heavy metals, phenolic compounds and textile dyes from industrial waste water using phosphonium based ionic liquids. *J Mol Liq* 323:114645
- Uddin M, Rahman M, Rukanuzzaman M, Islam M (2017) A potential low cost adsorbent for the removal of cationic dyes from aqueous solutions. *Appl Water Sci* 7(6):2831–2842
- Wang Z, Chen C, Liu H, Hrynsphan D, Savitskaya T, Chen J, Chen J (2020) Enhanced denitrification performance of *Alcaligenes* sp. TB by Pd stimulating to produce membrane adaptation mechanism coupled with nanoscale zero-valent iron. *Sci Total Environ* 708:135063
- Wang S, Gao H, Fang L, Hu Q, Sun G, Chen X, Yu C, Tang S, Yu X, Zhao X (2021) Synthesis of novel CQDs/CeO₂/SrFe₁₂O₁₉ magnetic separation photocatalysts and synergic adsorption-photocatalytic degradation effect for methylene blue dye removal. *Chem Eng J Adv* 6:100089
- Wang Z, Hu L, Zhao M, Dai L, Hrynsphan D, Tatsiana S, Chen J (2022) Bamboo charcoal fused with polyurethane foam for efficiently removing organic solvents from wastewater: experimental and simulation. *Biochar* 4(1):1–16
- Wang L, Du Yu, Zhu Q, Song J, Ou K, Xie G, Yu Z (2023) Regulating the alkyl chain length of quaternary ammonium salt to enhance the inkjet printing performance on cationic cotton fabric with reactive dye ink. *ACS Appl Mater Interfaces* 15(15):19750–19760
- Wu M, Wang Y, Lu B, Xiao B, Chen R, Liu H (2021a) Efficient activation of peroxymonosulfate and degradation of Orange G in iron phosphide prepared by pickling waste liquor. *Chemosphere* 269:129398
- Wu Z, Dong J, Yao Y, Yang Y, Wei F (2021b) Continuous flowing electrocoagulation reactor for efficient removal of azo dyes: kinetic and isotherm studies of adsorption. *Environ Technol Innov* 22:101448
- Xing Y, Luo X, Liu S, Wan W, Huang Q, Chen W (2021) A novel eco-friendly recycling of food waste for preparing biofilm-attached biochar to remove Cd and Pb in wastewater. *J Clean Prod* 311:127514
- Xu X, Xu Z, Huang J, Gao B, Zhao L, Qiu H, Cao X (2021) Sorption of reactive red by biochars ball milled in different atmospheres: co-effect of surface morphology and functional groups. *Chem Eng J* 413:127468
- Yamada I, Kataoka T, Ikeda R, Samitsu S, Tagaya M (2022) Effective immobilization of monomeric methylene blue on hydroxyapatite nanoparticles by controlling inorganic-organic interfacial interactions. *Inorg Chem* 61(12):4865–4878
- Yao Y, Gao B, Fang J, Zhang M, Chen H, Zhou Y, Creamer AE, Sun Y, Yang L (2014) Characterization and environmental applications of clay-biochar composites. *Chem Eng J* 242:136–143
- Zahedifar M, Seyedi N, Shafiei S, Basij M (2021) Surface-modified magnetic biochar: highly efficient adsorbents for removal of Pb(II) and Cd(II). *Mater Chem Phys* 271:124860
- Zhang G, Zhao Z, Yin XA, Zhu Y (2021) Impacts of biochars on bacterial community shifts and biodegradation of antibiotics in an agricultural soil during short-term incubation. *Sci Total Environ* 771:144751
- Zhao J, Liang G, Zhang X, Cai X, Li R, Xie X, Wang Z (2019) Coating magnetic biochar with humic acid for high efficient removal of fluoroquinolone antibiotics in water. *Sci Total Environ* 688:1205–1215
- Zhou X, Liu Y, Zhou J, Guo J, Ren J, Zhou F (2018) Efficient removal of lead from aqueous solution by urea-functionalized magnetic biochar: preparation, characterization and mechanism study. *J Taiwan Inst Chem Eng* 91:457–467

Publisher's Note Springer Nature remains neutral with regard to jurisdictional claims in published maps and institutional affiliations.